Octadentate Bispidine Chelators for Tb(III) Complexation: Pyridine Carboxylate versus Pyridine Phosphonate Donors

Lucas Petitpoisson, Anli Mahamoud, Valérie Mazan, Maryame Sy, Olivier Jeannin, Eva Tóth, Loïc J Charbonnière, Mourad Elhabiri, Aline M Nonat

Octadentate bispidine chelators for Tb(III) complexation: pyridine carboxylate *versus* pyridine phosphonate donors

Lucas Petitpoisson,[a‡] *Anli Mahamoud,*[a‡] *Valérie Mazan,*[b] *Maryame Sy,*[a] *Olivier Jeannin,*[c] *Eva Tóth,*[d] *Loïc J. Charbonnière,*[a] *Mourad Elhabiri,*[b] *Aline M. Nonat,*[a*]

[a] Equipe de Synthèse pour l'Analyse, Université de Strasbourg, CNRS, IPHC UMR 7178, F-67 087 Strasbourg, France. Email: aline.nonat@unistra.fr

[b] Université de Strasbourg/CNRS/UHA, UMR7042, Laboratoire d'Innovation Moléculaire et Applications (LIMA), Team Bio(IN)organic and Medicinal Chemistry, European School of Chemistry, Polymers and Materials (ECPM), 25 Rue Becquerel, F-67087 Strasbourg, France.

[c] Institut des Sciences Chimiques de Rennes, UMR-CNRS 6226, 263 Avenue du Général Leclerc, CS 74205, F-35042 Rennes Cedex, France.

[d] Centre de Biophysique Moléculaire, CNRS UPR 4301, Université d'Orléans, Rue Charles Sadron, F-45071.

‡ These authors have contributed equally to this work.

KEYWORDS: bispidine / terbium / lanthanide / medical imaging probes / luminescence

ABSTRACT

With their rigid and preorganized skeleton, bispidine (3,7-diazabicyclo[3.3.1]nonane) chelators are very appealing for the preparation of metal complexes with high kinetic inertness. In the aim to develop new Tb(III)-based medical imaging probes, this study describes the synthesis and the physico-chemical properties of two novel terbium(III) complexes with octadentate bispidine-based ligands substituted with either pyridine-phosphonate ($H_6\mathbf{L^1}$) or picolinate ($H_4\mathbf{L^2}$) subunits. Thermodynamic stability constants of the corresponding Tb(III) complexes have been determined by potentiometric, UV-visible absorption spectrophotometric and spectrofluorimetric methods. Despite their apparent similarity, these two octadentate ligands differ in their most stable conformation: *chair-chair* conformation for $H_4\mathbf{L^2}$ and *boat-chair* conformation for $H_6\mathbf{L^1}$, as confirmed by ^{1}H NMR studies and suggested from physico-chemical investigations. This conformation change induces different protonation schemes for the two ligands. The kinetic inertness of the Tb complexes has been studied in various media and assessed by transmetallation and transchelation experiments. In particular, Tb($\mathbf{L^2}$) displayed a remarkable kinetic inertness with no measurable dissociation over two months in mouse serum at 10^{-5} M concentration. The complex was also very inert in the presence of 50-fold excess of Zn(II) in H_2O at pH = 7.4 (7% of dissociation over two months). The complexes with ligand $\mathbf{L^1}$ are significantly less inert, emphasizing the influence of the ligand conformation on the kinetic inertness of the Ln(III) complexes. Finally, the luminescence properties of the isolated complexes have also been investigated. A bright green luminescence was observed, especially for Tb($\mathbf{L^2}$) which displays a high quantum yield value of 50% in H_2O (60% in D_2O; λ_{exc} = 263 nm). In addition, luminescence lifetimes of 1.9(2) ms and 1.7(2) ms have been measured for Tb($\mathbf{L^1}$) and Tb($\mathbf{L^2}$), respectively, hence confirming the formation of nona-coordinated complexes with one inner-sphere water molecule. These data on a bispidine scaffold pave the way for developing bright, inert luminescent probes for bioimaging and for radiolabeling applications with Tb(III) radioisotopes.

Introduction

With their unique magnetic[1] and optical properties,[2] as well as the availability of radioisotopes of high interest for nuclear medicine,[3] trivalent lanthanides ions (Ln(III)) play a key role in the development of biomedical imaging and therapy.[4] For four decades, the unique magnetic properties of Gd^{3+}, attributed to its high electron spin and slow electronic relaxation, have made

it a cornerstone for the development of magnetic resonance imaging (MRI) contrast agents, the market leader being $[Gd(DOTA)]^-$ (DOTA = (1,4,7,10-tetraazacyclododecane-1,4,7,10-tetraacetic acid)).[5,6,7] In addition, nearly all Ln(III), except for La(III) and Lu(III), exhibit characteristic line-like emission spectra spanning from ultraviolet (UV) to near-infrared (NIR) that have promoted the establishment of lanthanide complexes and their nanoparticles as bright luminescent tags or sensors for various imaging applications.[8] More recently, the development of targeted radioimmunotherapy (RIT), associated with immuno Positron Emission Tomography (immuno-PET), has prompted experts to develop and use radiopharmaceuticals with long radioactive half-lives, compatible with the slow biodistribution pharmacokinetics of macromolecules such as antibodies.[9,10,11] In this regard, some lanthanides, and particularly Tb(III), Ho(III), and Lu(III) have radioisotopes with suitable radiation energies and decay properties for the development of diagnostic and therapeutic radiopharmaceuticals.[12,13] Among these, Tb(III) plays a crucial role and is often described as the "*Swiss Army knife*" for nuclear imaging and therapy.[14,15,16,17] Indeed, ^{152}Tb (β^+) and ^{155}Tb (γ) are excellent candidates for PET and SPECT, with half-lives of 17.5 hours and 5.3 days, respectively. Meanwhile, ^{149}Tb and ^{161}Tb are promising candidates for α and β^- radiation therapy. Combined with specific targeting, the use of ^{161}Tb or a cocktail of Tb^{III} isotopes allows the creation of theranostic probes, enabling both therapy and imaging control in a single injection, thus offering promising prospects in the field of nuclear and personalized medicines.

For all these applications, lanthanide ions must be coordinated as thermodynamically stable and kinetically inert complexes to prevent the release of free Ln(III) and its nonspecific deposition in tissues.[18,19] Numerous chelators, often macrocyclic ligands with coordinating pendant arms, have been developed so far.[20,21,22,23] DOTA and its derivatives have been successfully used for the complexation of Gd(III) as well as for radiolabelling with ^{90}Y, ^{177}Lu, and ^{161}Tb.[24,25,26] However, its kinetics of complexation is slow and this ligand lacks a chromophoric antenna for the sensitization of Ln(III) luminescence. In the field of MRI, the kinetic inertness of Gd(III) complexes is also questioned, as free Gd(III) released has been shown to result in accumulation in muscles and brain.[27] Repeated injections have been shown to cause a disease called Nephrogenic Systemic Fibrosis in patients suffering from renal impairment.[7] For all these reasons, novel ligand designs are still needed to meet the simultaneous requirements of fast complexation kinetics under mild conditions for immuno-PET, efficient luminescent sensitization, and, very importantly, very strong kinetic inertness to avoid toxicity at high doses as well as to prevent nonspecific signals and irradiation in the case of nuclear imaging and therapy.

Pyclen (3,6,9,15-tetraazabicyclo[9.3.1]pentadeca-1(15),11,13-triene)-based ligands, substituted with picolinate antennae, have recently been shown to form very bright luminescent complexes with quantum yields up to 95%. These complexes exhibit fast complexation kinetics, enabling radiolabelling with both ^{161}Tb and ^{177}Tb at 50 MBq/nmol, with radiochemical yields (RCY) exceeding 90% ratio (50 MBq and 1:14 M:L ratio). Under the conditions of the study, the radiolabelled complexes displayed remarkable kinetic inertness, with more than 90% of the intact complex after 7 days in saline solutions and PBS.[28] Bispidine (3,7-diazabicyclo[3.3.1]nonane) is another azamacrobicyclic scaffold which can be substituted at various positions in order to form rigid complexes with usually a good kinetic inertness. In particular, remarkably inert Mn(II)[29,30] and ^{64}Cu(II) complexes have been reported.[31,32,33]

A few examples of lanthanide complexes with bispidine-type ligands have already been reported. In particular, ligands **bispa**[34] and **L**[7 35] (Figure 1) have been proven to complex Ln(III), showing good luminescent properties of the Tb(III) complexes, as well as excellent radiolabelling capacities with ^{177}Lu.[36,37] Nevertheless, the presence of the methyl ester group significantly affects the solubility of the ligands and of their complexes, as well as their protonation and complexation schemes. In addition, they are prompted to hydrolysis *in vivo*. As part of our ongoing research on Ln(III), we herein describe a comparison between picolinate and pyridine-phosphonate substitution[38] as this coordinating group has previously demonstrated to promote higher thermodynamic stability and kinetic inertness when incorporated into polyazamacrocycles such as tacn and pyclen.[39]

This strategy was applied to the bispidine skeleton and the structural properties of the picolinate (**L**^{1}) and pyridine-phosphonate (**L**^{2}) ligands, their protonation properties as well as the stability constants and luminescent properties of the corresponding Tb(III) complexes were compared. Finally, the kinetic inertness of the corresponding complexes in various media was monitored and compared. For all these features, the relationships between the structure and properties are discussed.

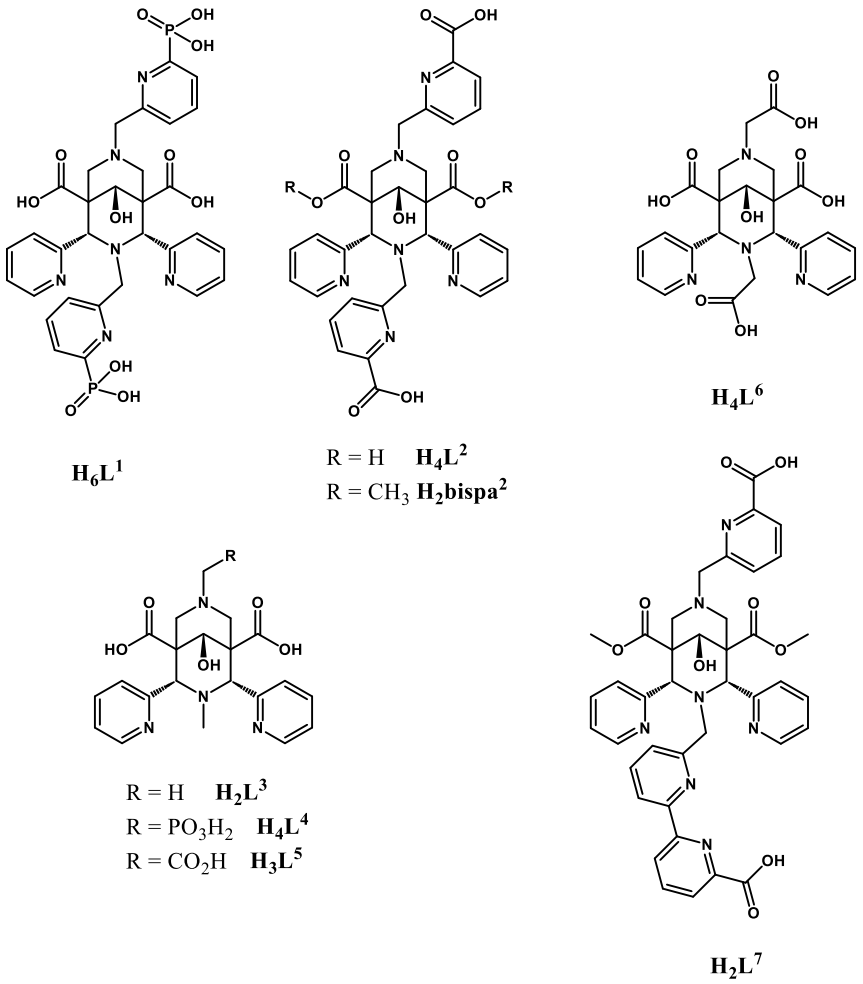

Scheme 1. Chemical structures of the ligands $H_6\mathbf{L}^1$, $H_4\mathbf{L}^2$, the dimethyl reference compound $H_2\mathbf{L}^3$ and reference compounds (H_2**bispa**[35], $H_4\mathbf{L}^4$,[30] $H_3\mathbf{L}^5$,[40] $H_4\mathbf{L}^6$ [40] and $H_2\mathbf{L}^7$ [36]).

Experimental Section

General procedures. Solvents and starting materials were purchased from Aldrich, Acros, Fluorochem, TCI chemicals and Alfa Aesar and were used without further purification, unless stated otherwise. Solvents for high-performance liquid chromatography (HPLC) were HPLC-grade. All aqueous solutions were prepared with Milli-Q water ($\rho < 18M\Omega$). $TbCl_3.6H_2O$ (99.9%) was obtained from Sigma-Aldrich. Intermediate **3** (dimethyl (2R,4S,9r)-9-hydroxy-3-methyl-2,4-di(pyridin-2-yl)-3,7-diazabicyclo[3.3.1]nonane-1,5-dicarboxylate) was obtained according to previously reported procedures.[30]

^1H, ^{13}C and ^{31}P NMR spectra and 2D COSY, NOESY and HSQC experiments were recorded on Bruker Avance 400 and Avance 500 spectrometers. ^{13}C and ^{31}P NMR spectra were measured

with ^{1}H decoupling. All chemical shifts (δ) values are given in part per million and are referenced to the solvent.[41] When unspecified, coupling constants refer to H–H coupling. The given pH values are corrected for the deuterium isotopic effects (pD = apparent pH + 0.4).[42]

Maldi-tof measurements were carried out on an Autoflex TM MALDI-TOF mass spectrometer (Bruker Daltonics GmbH, Bremen, Germany). This instrument was used at a maximum accelerating potential of 20 kV in positive mode and was operated in linear mode. The delay extraction was fixed at 560 ns and the frequency of the laser (nitrogen 337 nm) was set at 5 Hz. The acquisition mass range was set to 1500-10000 m/z with a matrix suppression deflection (cut off) set to 1500 *m/z*. The equipment was calibrated with ACTH_1-17 ($[M+H]^+$ 2094.42), insulin ($[M+H]^+$ 5732.52), ubiquitin I ($[M+H]^+$ 8565.76) and myoglobin ($[M+H]^+$ 16952.31). Each raw spectrum was opened with flexAnalysis 2.4 build 11 (Bruker Daltonics GmbH, Bremen, Germany) software and processed using the following parameters: signal-to-noise threshold of 1, Savitzky-Golay algorithm for smoothing, median algorithm for baseline substraction.

High Performance Liquid Chromatography/UV absorption spectrophotometry analysis was performed on an Agilent 1100 system equipped with a Diode-Array Detector. Samples (10 µL) were injected into the column (Uptisphere® CS Evolution™ C18AQ, 250 x 4.6 mm, 5 µm, Interchim) at room temperature. The pH value of the samples was adjusted to 7.4 prior their injection. A water/methanol gradient was used for mobile phase as follows: 100% of water from 0 to 5 min post injection, linear increase to 70% MeOH at 10 min, linear increase to 100% MeOH at 15 min, followed by a linear decrease to 100% water at 20 min before the next run. The flowrate was 1 mL/min. λ = 254 nm was used for the detection.

Elemental analyses and electrospray mass spectrometry analysis were carried out by the Service Commun d'Analyses of the University of Strasbourg.

Synthesis of the ligands

Compound 3 ($C_{21}H_{24}N_4O_5$, 412.45 g.mol^{-1}). Compound **1** (0.6 g, 1.07 mmol, 1 equiv) was dissolved in anhydrous tetrahydrofuran (THF, 30 mL) and cooled at -78°C. Then, sodium borohydride (30 mg, 0.8 mmol, 0.75 equiv) was added by portion. After 2 h, the reaction was completed as indicated by ^{1}H NMR measurement. Ammonium chloride (pH 5, 17 mL) was added under stirring. Then, water (50 mL) was added, the aqueous phase was extracted by dichloromethane (DCM, 3 x 30 mL), and the organic phase was dried over $MgSO_4$. Finally, the solvent was removed under reduced pressure. The crude intermediate **2** was solubilized in 18

mL of DCM, and trifluoroacetic acid (4.1 mL) was added. The solution was stirred at 50°C overnight. Then, the reaction mixture was concentrated under vacuum, the residue was dissolved in methanol (MeOH) and the purple solution was stirred at 65°C for 1 h. Subsequently, the hot suspension was filtered and the filtrate was concentrated to dryness. Then, the crude residue was purified by flash column chromatography (SiO_2, DCM/MeOH from 100/0 to 85/15 in 30 min). The pure compound **3** was obtained as a white solid (234 mg, 53% over two steps). TLC (DCM/MeOH - 90/10) R_f = 0.39; **^{1}H NMR** (400 MHz, 25°C, $CDCl_3$): δ 3.49 (s, 2H, 2/4), 3.55 (d, $J_{H6ax8ax}$ = 13.2 Hz, 2H, $6_{ax}/8_{ax}$), 3.61 (s, 6H, OCH_3, 16), 4.03 (d, $J_{H6eqH8eq}$ = 13.2 Hz, 2H, $6_{eq}/8_{eq}$), 4.64 (s, 1H, 9), 5.33 (s, 2H, 3/7), 7.18 (ddd, $^3J_{HH}$ = 6.7 Hz, $^3J_{HH}$ = 4.9 Hz, $^4J_{HH}$ = 1.2 Hz, 2H, b), 7.46 (d, $^2J_{HH}$ = 7.8 Hz, 2H, d), 7.71 (td, $^3J_{HH}$ = 7.7 Hz, $^4J_{HH}$ = 1.8 Hz, 2H, c), 8.63 (m, 2H, a); **^{13}C NMR** (126 MHz, 25°C, DMSO-d_6): δ 48.32 (8 and 6), 51.82 (10), 57.89 (2 and 4), 73.78 (9), 122.73 (b), 124.45 (d), 136.48 (c), 148.32 (a), 159.09 (C_{quat}), 171.33 (CO) ppm**.**

Ligand H_6L^1 ($C_{31}H_{32}N_6O_{11}P_2$, 726.58 g.mol^{-1}). To a solution of compound **3** (0.189 g, 0.46 mmol, 1 equiv) in anhydrous acetonitrile (CH_3CN, 50 mL) were added diethyl (6-(chloromethyl)pyridin-2-yl)phosphonate (0.266 g, 1.01 mmol, 2.2 equiv) and K_2CO_3 (0.140 g, 1.01 mmol, 2.2 equiv) under inert atmosphere. After, the mixture was stirred at 40°C for 24 h, the solution was filtered, then the product was dried under vacuum. The crude intermediate **6** was used without further purification. The solid was dissolved in 6M HCl (30 mL), and the mixture was heated at 60°C for 3 days. Subsequently, the solvent was evaporated, and the product was purified by FPLC (C_{18}, using H_2O/CH_3CN from 100/0 to 0/100) to give **8^1** and **8^2**. The mixture of intermediate **8** was dissolved in water (11 mL) and the pH adjusted to 13 with lithium hydroxide, then THF (7 mL) was added and the mixture was stirred for 16h at room temperature. The solvent was evaporated, and the product purified by FPLC (C_{18}, H_2O/CH_3CN with 0.1% of TFA from 100/0 to 0/100) to give H_6**L^1•2 TFA** (0.134 g) as an off-white powder with 30% yield over two steps. TLC (MeOH/H_2O 10/90); R_f = 0.26; ^{1}H NMR (500 MHz, D_2O, pD 12.1) δ = 2.20 (d, $J_{H6axH8ax}$= 12.6 Hz, 2H, $6_{ax}/8_{ax}$), 2.89 (d, $J_{H6eqH8eq}$ = 12.5 Hz, 2H, $6_{eq}/8_{eq}$), 3.49 (s, 2H, 11), 3.54 (s, 2H, 12), 3.96 (s, 1H, 9), 5.16 (s, 2H, 2/4), 7.12 (d, ^3J = 7.1 Hz, 1H, g), 7.18 – 7.23 (m, 2H, b/b'), 7.24 – 7.26 (m, 1H, j), 7.34 (d, ^3J = 7.6 Hz, 2H, d/d'), 7.57 – 7.64 (m, 2H, f and e), 7.64 – 7.70 (m, 2H, c/c'), 7.71 – 7.77 (m, 1H, h), 7.83 – 7.89 (m, 1H, i), 8.43 – 8.53 (m, 2H, a/a'); ^{13}C NMR (125 MHz, D_2O, pD 12.1) δ = 51.8 (1/5), 56.5 (11), 56.9 (6/8), 62.8 (2/4), 65.4 (c/c'), 74.1 (9), 122.7 (b/b'), 124.2 (g), 124.4 (e and f), 124.9 (j), 125.1 (h), 126.5 (d), 136.9 (i), 137.0 (C_{quat}), 149.4 (a), 158.8 (C_{quat}), 158.9 (C_{quat}), 163.1 (C_{quat}), 178.9

(C_{quat}); MS^+ (MALDI-TOF, matrix: α-cyano-4-hydroxycinnamic acid): *m/z* =727.348 $[M + H]^+$; Elemental analysis: calculated for H_6**L^1•2 TFA**, % C 44.36, % H 4.01, % N 8.92. Found % C 44.04, % H 3.59, % N 8.80; retention time was 13.30 min on standard analytical HPLC method (Uptisphere® CS Evolution^{TM} C18AQ, H_2O/CH_3OH).

Ligand H_4L^2 ($C_{33}H_{30}N_6O_9$, 654.64 g.mol^{-1}). Compound **3** (334 mg, 0.81 mmol, 1 equiv.) was dissolved in anhydrous CH_3CN (30 mL) with K_2CO_3 (268 mg, 1.94 mmol, 2.4 equiv.) under inert atmosphere. Then 2-(chloromethyl)picolinate (360 mg, 1.94 mmol, 2.4 equiv.) was added with a small amount of KI and the mixture was heated at 40°C for 24 h. Subsequently, K_2CO_3 was filtered, and the solvent was removed under vacuum. The crude product was then used for the next step without purification and dissolved in 14 mL of H_2O/THF (4/3). LiOH (146 mg, 6.1 mmol, 10 equiv) was added and the solution was stirred for 16 h at room temperature. The crude residue was purified by FPLC (C_{18}AQ, H_2O/CH_3CN from 100/0 to 0/100) to give H_4**L^2** (295 mg) as an off-white powder with 56% yield. TLC (MeOH/H_2O 10/90); R_f = 0.28; ^{1}H NMR (DMSO- d_6, 400 MHz): δ = 3.27 (s, 2H, 11), 3.50 (d, $J_{H6axH8ax}$ = 11.4 Hz, 2H, $6_{ax}/8_{ax}$), 4.00 (d, $J_{H6eqH8eq}$ = 11.9 Hz, 2H, $6_{eq}/8_{eq}$), 4.16 (s, 1H, 9), 4.56 (s, 2H, 12), 5.08 (s, 2H, 2/4), 7.07 (d, ^3J = 7.5 Hz, 1H, h), 7.12 (dd, ^3J = 7.2 Hz, ^3J = 5.2 Hz, 2H, b/b'), 7.41 (d, ^3J = 7.6 Hz, 2H, d/d'), 7.61 (t, ^3J = 7.7 Hz, 2H, c/c'), 7.69 – 7.80 (m, 2H, i and j), 8.01 (d, ^3J = 4.2 Hz, 2H, a/a'), 8.06 (d, ^3J = 7.3 Hz, 1H, e), 8.22 – 8.34 (m, 2H, f and g); ^{13}C NMR (DMSO-d_6, 125 MHz) δ = 48.9 (C_{quat}), 56.0 (6/8), 57.2 (11), 60.9 (12), 64.3 (2/4), 72.8 (9), 122.4 (j), 122.8 (b/b'), 124.9 (g), 126.8 (h), 127.4 (d/d'), 129.0 (e), 136.3 (c/c'), 136.9 (i), 138.8 (f), 146.9 (C_{quat}), 148.2 (a/a'), 149.1 (C_{quat}), 151.2 (C_{quat}), 156.7 (C_{quat}), 157.2 (C_{quat}), 165.9 (C_{quat}), 166.0 (C_{quat}), 170.5 (C_{quat}); MS^+ (MALDI-TOF, matrix: α-cyano-4-hydroxycinnamic acid): *m/z* = 655.77 $[M + H]^+$; Elemental Analysis: Calculated for H_4**L^2•1.5 H_2O**, %C 58.15, %H 4.88, %N 12.33. Found: %C 57.91, %H 4.78, %N 12.53; retention time was 7.46 min on our standard analytical HPLC method (Uptisphere® CS Evolution^{TM} C_{18}AQ, H_2O/CH_3OH).

Ligand H_2L^3 ($C_{21}H_{24}N_4O_5$, 412.44 g.mol^{-1}). K_2CO_3 (40 mg, 0.29 mmol, 2.4 equiv.) was added to a solution of compound **3** (50 mg, 0.12 mmol, 1 equiv.) in anhydrous CH_3CN (6 mL) under inert atmosphere. Then, iodomethane (15 µL, 0.24 mmol, 2.0 equiv.) was added and the mixture was heated at 80 °C for 72 h. Subsequently, K_2CO_3 was filtered and the solvent was removed under vacuum. The crude product was then used for the next step without purification and dissolved in a mixture of 7.5 mL of H_2O/THF (3/2). LiOH (14 mg, 0.58 mmol, 4.8 equiv.) was then added. The solution was stirred for 16 h at room temperature. The crude residue was purified by FPLC (C18AQ, 100/0 H_2O/CH_3CN to 100% CH_3CN with 0.1% TFA) to give

compound H_2**L^3•2 TFA•H_2O** (47 mg) as an off-white powder with 59% yield. TLC (MeOH/H_2O 10/90); R_f = 0.14. ^{1}H NMR (D_2O, 400 MHz): δ = 1.66 (s, 3H, 14), 1.90 (d, $J_{H6axH8ax}$ = 12.2 Hz, 2H, $6_{ax}/8_{ax}$) 2.10 (s, 3H, 15), 2.81 (d, $J_{H6eqH8eq}$ = 12.1 Hz, 2H, $6_{eq}/8_{eq}$), 3.84 (s, 1H, 9), 4.37 (s, 2H, 2/4), 7.22 (ddd, 2H, ^3J = 7.6 Hz, ^3J = 4.9 Hz, ^4J = 1.2 Hz, b/b'), 7.30 (d, 2H, ^3J = 7.8 Hz, d/d'), 7.64 (td, 2H, ^3J = 7.7 Hz, ^4J = 1.8 Hz, c/c'), 8.49 (dd, 2H, ^3J = 4.6 Hz, ^4J = 1.5 Hz, a/a'). ^{13}C NMR (D_2O, 100 MHz): δ = 43.2 (14), 45.9 (15), 51.6 (C_{quat}), 58.4 (6/8), 67.7 (2/4), 74.1 (9), 122.8 (b/b'), 126.0 (d/d'), 137.0 (c/c'), 149.2 (a/a'), 159.8 (C_{quat}), 179.0 (C_{quat}); MS^+ (MALDI-TOF, matrix: α-cyano-4-hydroxycinnamic acid): *m/z* = 413.49 $[M + H]^+$; Elemental Analysis: Calculated for H_2**L_3 • 2 TFA • H_2O**, %C 45.60, %H 4.29, %N 8.51. Found: %C 45.63, %H 4.09, %N 8.39; retention time was 13.9 min on our standard analytical HPLC method (Uptisphere® CS Evolution™ C18AQ, H_2O/CH_3OH).

Synthesis of the Tb(III) Complexes

General procedure: To an aqueous solution of the ligand, 1.1 equivalent of $TbCl_3.6H_2O$ was added. Then, the pH was adjusted to 7.4 with a 1M LiOH solution. The solution was heated under stirring at 50°C for 30 min, and the formation of complex was followed by HPLC (H_2O/MeOH). The solvent was then evaporated under vacuum, and the product was purified by FPLC (C_{18}, using H_2O/MeOH from 100/0 to 0/100) to give the pure final complex.

[TbL^1] ($C_{31}H_{30}N_6O_{11}P_2Tb$, 882.47 gmol^{-1}). H_6**L^1•3.5 MeOH** (20 mg, 0.0243 mmol, 1 equiv) and $TbCl_3.6H_2O$ (7 mg, 0.027 mmol, 1.1 equiv) to give pure **[TbL^1]** as an off-white powder (15 mg, 60%); Elemental analysis: calculated for **[TbL^1]•MeOH•7 H_2O**: % C 36.90, %H 4.64, %N 8.07. Found % C 37.18, %H 4.41, %N 7.71; Retention time (C_{18}AQ, H_2O/MeOH, general method) was 4.2 min (Figure S19).

[TbL^2] ($C_{33}H_{36}Cl_3Li_3N_6O_{13}Tb$, 1010.78 gmol^{-1}). H_4**L^2•1.5 H_2O** (21 mg, 0.031 mmol, 1 equiv) and $TbCl_3.6H_2O$ (12.7 mg, 0.034 mmol, 1.1 equiv) to give pure **[TbL^2]** as a powder (22.8 mg, 73%); Elemental Analysis: Calculated for **[TbL^2]•3 LiCl•4 H_2O**, %C, 39.21, %H, 3.59, %N, 8.31. Found: %C, 39.54, %H, 3.74, %N, 8.38; Retention time (C_{18}AQ, H_2O/MeOH, general method) was 4.1 min (Figure S20).

NMR studies

11 mg of $H_6\mathbf{L^1}$•**2 TFA** was dissolved in 600 µL of D_2O ([$\mathbf{L^1}$] = 19.2 mM) and the pD was adjusted by addition of 5 µL of 40% NaOD solution in D_2O. Changes upon deprotonation from pD 2 to 12 were monitored by recording the ^1H (400 MHz) and ^{31}P (162 MHz) spectra.

Physicochemical and Spectrophotometric Studies

All aqueous solutions were prepared with water ChromasolvTM Plus for HPLC from Honeywell. All the stock solutions were prepared by weighing solid products using an ML304T100 Mettler Toledo analytical balance (precision 0.01 mg). Tb(III) solutions were prepared from their chloride salt ($TbCl_3 \cdot 6H_2O$, 99.9%, Sigma-Aldrich), and their concentrations were determined by colorimetric titrations with EDTA (10^{-2} M, Merck, Titriplex III) according to standard procedures using xylenol orange as indicator.[43]

Potentiometric Titrations

The potentiometric titrations of the free ligands $H_6\mathbf{L^1}$ (1.07 mM), $H_4\mathbf{L^2}$ (1.06 mM) and $H_2\mathbf{L^3}$ (1.64 mM) and of the Tb(III) complex of $\mathbf{L^2}$ ($[Tb(III)]_{tot}/[ligand]_{tot} = 1$) were performed using a Metrohm794 Basic Titrino automatic titrator system equipped with a combined glass electrode (Metrohm 6.0234.500, Long Life) filled with 0.1 M NaCl (Carlo-Erba-SDS Phar. Eur. 99–100.5%) in water and connected to a microcomputer (Tiamo light 1.2 program). The Tb(III)/ligand solutions were equilibrated for 20 min at 25°C prior to any measurement. The combined glass electrode was calibrated as a hydrogen concentration probe according to a procedure described elsewhere.[44] The potentiometric data of $H_6\mathbf{L^1}$, $H_4\mathbf{L^2}$ and $H_2\mathbf{L^3}$ ($H_2\mathbf{L^3}$ was used as a model; only the log K_H of the free ligand were determined) and their corresponding Tb(III) complexes (about 300 points collected over the pH range 2.5–11.5) were refined with the Hyperquad 2000 program.[45,46] At least three potentiometric titrations were treated as single sets, for each system. The quality of the fits was judged by the values of the sample standard deviation, S, and the goodness of fit, χ^2 (Pearson's test). At $\sigma_E = 0.1$ mV (0.023 σ_{pH}) and $\sigma_V = 5$ µL, the values of S in different sets of titrations were between 0.6 and 1.6 and χ^2 was below 99. The scatter of residuals vs pH was reasonably random, without any significant systematic trends, thus indicating a good fit of the experimental data (see supporting information). The stability and successive protonation constants were calculated from the cumulative constants determined with the program. The uncertainties in the log K values correspond to the added standard deviations in the cumulative constants.

Spectrophotometric Titrations vs pH of the Free Ligands

A 42.95 mL aliquot of solutions containing $H_6\mathbf{L^1}$ (50.0 μM), $H_4\mathbf{L^2}$ (35.5 μM) and $H_2\mathbf{L^3}$ (112.0 μM) were introduced in a jacketed cell (Metrohm) maintained at 25.0(2) °C (Lauda E200). The free hydrogen ion concentration was measured with a combined glass electrode (Metrohm 6.0234.500, Long Life) and a Metrohm 794 Basic Titrino automatic titrator system. The initial pH was adjusted to ~2.5–3.8 with standardized HCl (~0.1 mM), and the titrations of the ligands (2.5 < pH < 11.5) were then carried out by addition of known volumes of standardized NaOH solutions (~0.1 mM) using the automatic titrator system. After each addition and stabilization of the potential drift, an absorption spectrum was recorded using a Varian CARY 50 spectrophotometer fitted with Hellma optical fibres (Hellma, 041.002-UV) and an immersion probe made of quartz Suprasil (Hellma, 661.500-QX). The Varian CARY 50 spectrophotometer was interfaced (Cetrib) with the Basic Titrino 794 automatic titrator system allowing automatic absorption versus pH titrations.

Absorption and Emission Titrations of $H_6\mathbf{L^1}$ and $H_4\mathbf{L^2}$ by Tb(III) at pH 5.5

Stock solutions of $H_6\mathbf{L^1}$ (1.07 mM) and $H_4\mathbf{L^2}$ (1.06 mM) were prepared in acidic aqueous solutions. Several samples (2 mL) containing Tb(III):ligand ratios ranging from 0 to 5 were prepared with an aqueous solution buffered at pH 5.5 (20 mM MES buffer, 2-(N-morpholino)ethanesulfonic acid). The final concentrations of $H_6\mathbf{L^1}$ and $H_4\mathbf{L^2}$ were 52.5 μM and 106 μM, respectively while the concentration of the stock Tb(III) solution used to prepare these samples was 9.71 mM. The samples were kept overnight at 25 °C for equilibration. For each sample, a UV–vis absorption and an emission spectra (λ_{exc} = 268 nm) were recorded in 1 cm quartz Suprasil Hellma cell. Absorption spectra were recorded on a UV–vis–NIR Cary 5000 (Varian) spectrophotometer maintained at 25.0(2) °C. Emission spectra were recorded on Perkin Elmer LS50B.

Analysis and Processing of the Spectroscopic Data

The spectrophotometric data were analysed with Specfit[46,47,48] program which adjusts the absorptivities (or the intensity signals) and the stability constants of the species formed at equilibrium. Specfit uses factor analysis to reduce the absorbance (or emission intensity) matrix and to extract the eigenvalues prior to the multiwavelength fit of the reduced data set according to the Marquardt algorithm.[49] Specfit allowed the determination of the coordination model and of the stability constants of the formed Tb(III) species.

Photophysical Properties of the isolated TbL^1 and TbL^2 complexes in water at pH = 7

UV-visible absorption spectra were recorded on a Specord spectrometer from Jena Analytics. Steady state emission spectra were recorded on an Edinburgh Instrument FLP920 spectrometer working with a continuous 450 W Xe Lamp and a red sensitive R928 photomultiplier from Hamamatsu in Pelletier housing. All spectra were corrected for the instrumental functions. For emission spectra, a 330 nm cut-off filter was used to eliminate second order artefacts. Phosphorescence lifetimes were measured on the same instrument working in the Multi-Channel Spectroscopy (MCS) mode, using a Xenon flash lamp as the excitation source. Luminescence quantum yields of the Tb(III) complexes were measured according to conventional procedures,[50] with optically diluted solutions (absorbance < 0.05) using a bipyridine Tb(III) complex in water (Φ = 0.31) as reference.[51] The errors are estimated to be 10% on the lifetimes and 20% on the luminescence quantum yields. The hydration numbers of the complexes (q) were calculated from the luminescence lifetimes measured in H_2O and D_2O using the equation from reference.[52]

Kinetic inertness

The kinetic inertness of the isolated [Tb$\mathbf{L}^1$]Cl_3 and [Tb$\mathbf{L}^2$]Cl complexes was evaluated under different conditions. The complexes were tested: (a) in water at pH = 7.4; (b) in water at pH = 2; (c) in water with a 50-fold excess of Zn(II) at pH = 7.4; (d) in water with a 50-fold excess of Zn(II) at pH = 2; (e) in phosphate-buffered saline (PBS) at pH 7.4; and (f) diluted in mouse serum. For each of these conditions, 2 mL stock solutions of the Tb(III) complexes at 30 µM were prepared and incubated in a thermostat with agitation at 37°C for the total duration of the experiment, which lasted up to 2 months. The pH of each sample was monitored at the end of the period to ensure that it remained stable throughout the experiment.

At each time point (1h, 24 h, 48 h, 7 days, 14 days, 33 days, 51 days), 200 µL of each solution (conditions (a)-(e)) were dispensed into the wells of a 96-well microplate (Greiner Bio-One). The plate was equilibrated at room temperature for 5 mins and shaken for 1 min, and the emission spectra (λ_{exc} = 267 nm) were recorded using a TECAN Spark multimode microplate reader. The reader used a Xe flash lamp, an excitation bandwidth of 10 nm, a emission bandwidth of 5 nm, a delay time of 50 µs, and an integration time of 2 ms.

Crystallography

Data were collected on a APEX II Brucker AXS diffractometer with Mo–Kα radiation (λ = 0.71073 Å). Structure was solved by direct methods (SIR92)[53] and refined (SHELXL-2014/7)[54] by full-matrix least-squares methods as implemented in the WinGX software package.[55] An

empirical absorption (multi-scan) correction was applied. Hydrogen atoms were introduced at calculated positions (riding model) included in structure factor calculation but not refined with exception for the hydrogen atom on the secondary amino group (N2) whose coordinates have been freely refined (AFIX 2). Refinement parameters are summarized in table S1. Crystallographic data have been deposited to the Cambridge Crystallographic Data Center (CCDC 2209639).

Results and discussion

Synthesis of the ligands

The ligands $H_6\mathbf{L^1}$, $H_4\mathbf{L^2}$ and $H_2\mathbf{L^3}$ were obtained from the bispidol intermediate **3** (Scheme 2) whose synthesis has been slightly optimized for this study.[30,56,57] Indeed, it was observed that the addition of a highly concentrated TFA/DCM solution for deprotection led to partial degradation of the compound. Compound **3** was then engaged into nucleophilic substitution reactions with diethyl (6-(chloromethyl)pyridin-2-yl)phosphonate **4**, on the one hand, and 2-(chloromethyl)picolinate **5**, on the other hand, to afford compounds **6** and **7**, respectively. These intermediates were not isolated because their column chromatography resulted in significant yield decreases. Deprotection of the methyl ester function of the picolinate derivative **7** was straightforward in presence of LiOH yielding the final ligand $H_4\mathbf{L^2}$ in 74% over two steps from bispidol **3** after flash column chromatography on reverse phase C18 column. Deprotection of the phosphonic ester functions of compound **6** was achieved by heating in 6M HCl over 3 days at 55°C. These conditions were nevertheless not sufficient to fully hydrolyze the methyl ester functions and, consequently, a mixture of intermediates $\mathbf{8^1}$ and $\mathbf{8^2}$ was obtained, as indicated by ^{1}H NMR and MALDI-MS analyses of the crude mixture. Finally, complete saponification under basic conditions with LiOH was performed to yield pure $H_6\mathbf{L^1}$ ligand after flash column chromatography on reverse phase C18 column. The model ligand $H_2\mathbf{L^3}$ was obtained in 59 % yield according to a similar synthetic route (Scheme 2).

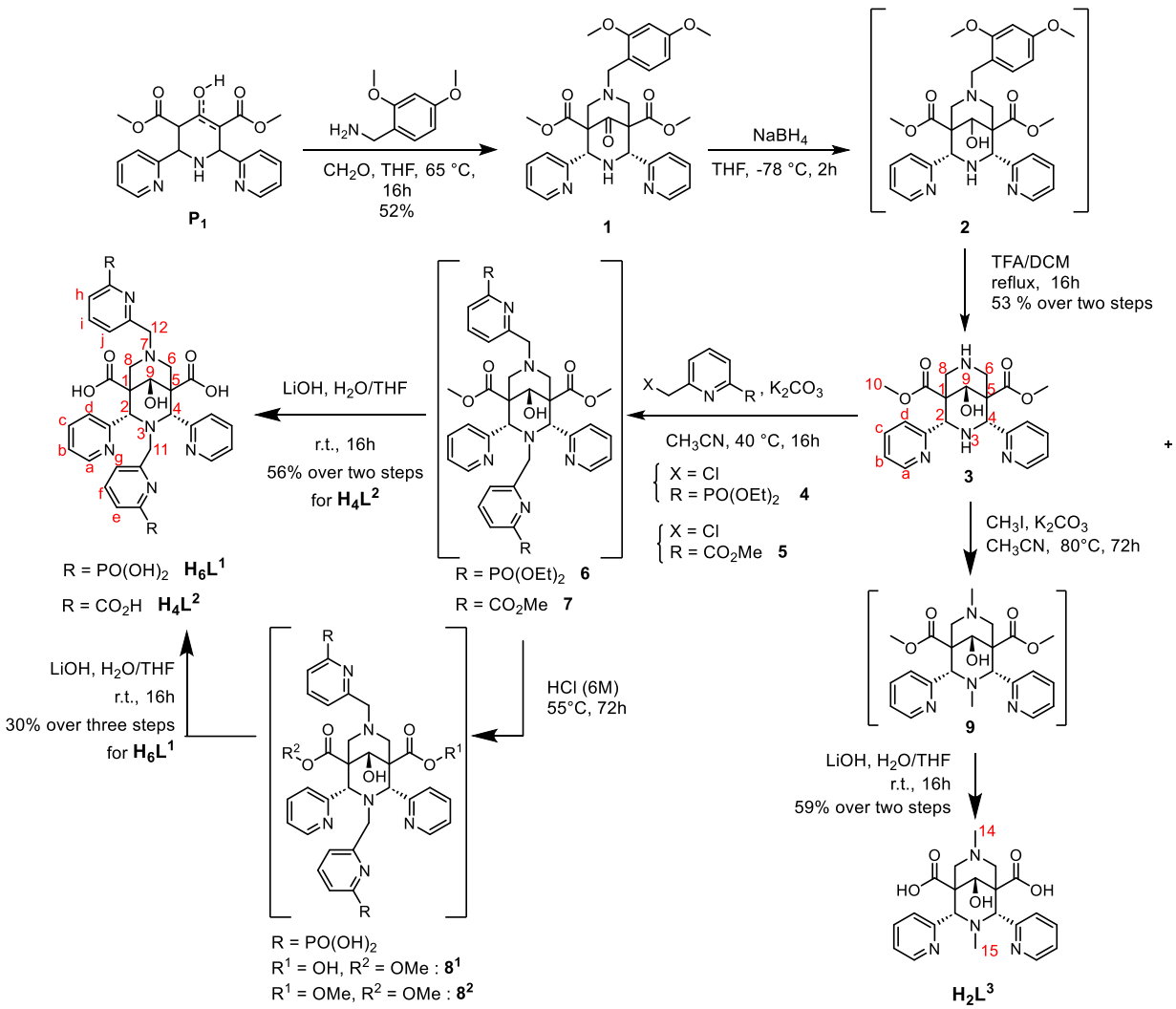

Scheme 2. Synthesis of ligands $H_6\mathbf{L}^1$, $H_4\mathbf{L}^2$ and $H_2\mathbf{L}^3$ and atom numbering for the NMR studies.

Such methodology is very encouraging for other substitutions of intermediate **3** paving the way for new paths from bispidone **1**. In addition, single crystals of the bispidone **1** were obtained by slow evaporation of a methanolic solution. The corresponding molecular structure (Figure 1) shows a chair-chair conformation of the bicyclic bispidine together with a *cis* configuration of the pyridyl rings, in agreement with literature data.[58] The chair-chair conformation is stabilized by a hydrogen bond involving the hydrogen atom of the secondary amine with the tertiary nitrogen N7 of the bispidine ($d_{H\ldots N7}$ = 2.2983(20) Å). The nitrogen N4 of one of the two pyridyl rings and the oxygen O6 of the methoxy group in *para* position of the benzyl ring are pointing toward the bispidine proton ($d_{H\ldots N7}$ = 2.4388(23) Å and $d_{H\ldots O6}$ = 2.7558 (21) Å suggesting a highly preorganized cavity suitable for metal complexation. Furthermore, the nitrogen of the second pyridyl is not pointing toward the complexation site as it is engaged in a intramolecular

N…C=O tetrel bond[59] with the π-hole of the neighboring carbonyl group ($d_{N3...C18}$ = 2.8488(23) Å). Crystallographic data are summarized in Table S1.

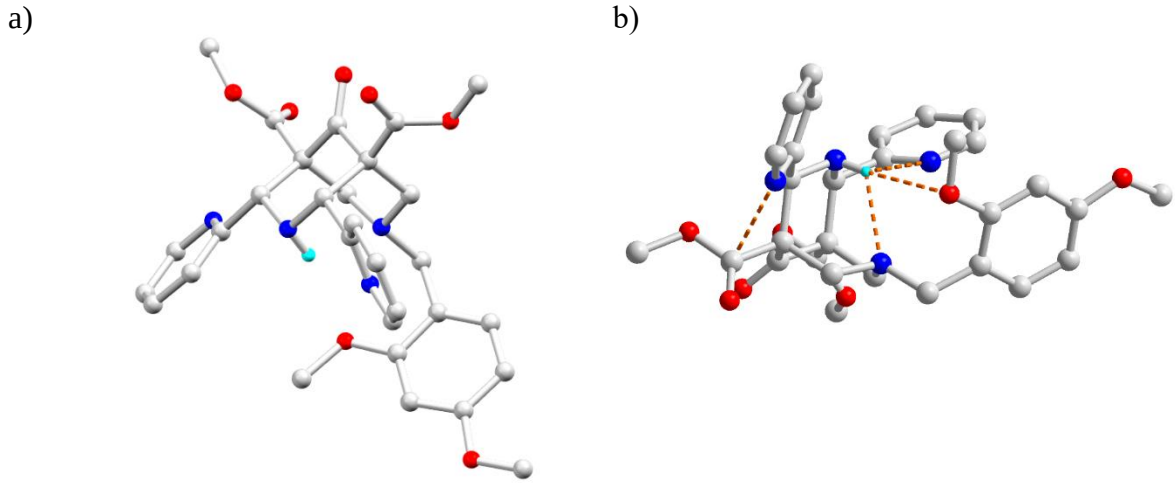

Figure 1. X-ray structure of bispidone **1** showing the bispidone scaffold (a) and the H-bond (b). H-atoms have been partially omitted for clarity.

The structures of the final ligands $\mathbf{L^1}$ and $\mathbf{L^2}$ have been confirmed by 1D and 2D ^{1}H NMR studies. In the case of ligand $\mathbf{L^2}$, the ^{1}H NMR spectrum recorded in D_2O and *d*$_6$-DMSO (Figure S10) is characteristic of a compound with a C_S symmetry and a typical Nuclear Overhauser Effect (NOE) is observed between H9 and $H6_{ax}$/$H8_{ax}$protons, which is characteristic of a chair-chair conformation with H9 pointing towards C6 and C8 (Figure 2). In the case of ligand $\mathbf{L^1}$, ^{1}H, ^{13}C and ^{31}P NMR spectra are quite intricate and strongly influenced by the presence of various protonated species (see below for NMR as a function of pD). However, the ^{31}P NMR spectrum recorded in excess of TFA clearly shows two unique singlets, confirming a single species in solution. At given pD values (pD = 6.5; pD = 12.1 for instance) a predominant species with 16 distinguishable protons is clearly seen (Figure S27), hence confirming C_S symmetry. The ^{1}H NMR spectra of ligands $\mathbf{L^1}$ and $\mathbf{L^2}$ are similar in many aspects. First, a NOE correlation is observed between H9 and $H6_{ax}$/$H8_{ax}$ of ligand $\mathbf{L^1}$, indicating the same orientation of the OH group towards C6 and C8 and therefore a chair-like conformation of the piperidine ring (Figure 2). Furthermore, for both ligands, correlations are also seen between the protons H2 or H4 of the other piperidine ring and the methylene protons of the substituent at N3 (H11) as well as with the H_d protons of the pyridyl substituents at C2 and C4. Nevertheless, it should be noted that the spectra of the two ligands diverge in the two following aspects. Firstly, a weak W shaped ^4J coupling is seen between the protons H2/H4 and the protons $H6_{ax}$/$H8_{ax}$ for the picolinate derivative $\mathbf{L^2}$ while no such coupling is observed for $\mathbf{L^1}$. This W coupling is typical of bispidol in chair-chair conformation.[32] Secondly, an additional NOE can be seen between the

protons H2/H4 and the H_g protons of the pyridine-phosphonate substituent at N3. Such coupling would be enhanced if the C2/C4 piperidine ring is in a boat conformation, which would also explain the lack of W coupling with $H6_{ax}/H8_{ax}$ or $H6_{eq}/H8_{eq}$. In the following, we will thus assume that ligand $\mathbf{L^1}$ is in the boat-chair conformation (Figure 2).

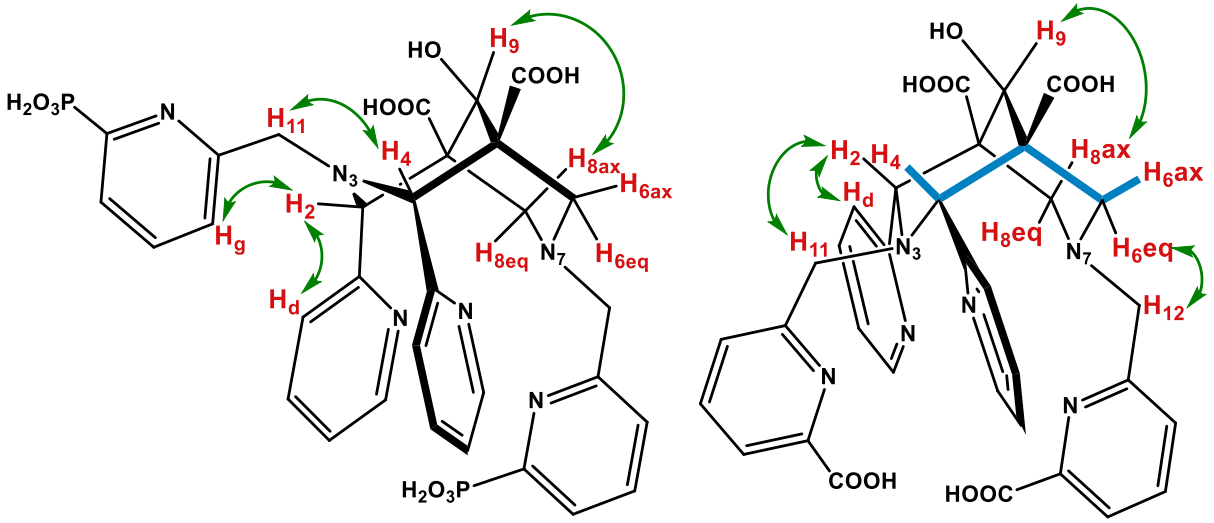

Figure 2. Schematic representation of the stereochemistry of ligands $H_6\mathbf{L^1}$ (left) and $H_4\mathbf{L^2}$ (right) showing W coupling in ^{1}H-^{1}H NMR COSY (W) and NOE interactions in ^{1}H-^{1}H NMR ROESY experiments (↻).

Protonation Properties of the Ligands

The fully deprotonated species $(\mathbf{L^1})^{6-}$ and $(\mathbf{L^2})^{4-}$ display in total 12 and 10 protonation sites, respectively: two bispidine tertiary amino functions and four N-pyridines respectively for $(\mathbf{L^1})^{6-}$ and $(\mathbf{L^2})^{4-}$, two phosphonate PO_3^{2-} units and two carboxylate units for $(\mathbf{L^1})^{6-}$ and four carboxylate units for $(\mathbf{L^2})^{4-}$. Hence, determining this intricate protonation scheme of both ligands and the corresponding protonation constants log K_H is a prerequisite for the study of the thermodynamic stability of the targeted Tb(III) complexes. In this study, the protonation constants of ligands $H_6\mathbf{L^1}$, $H_4\mathbf{L^2}$ and $H_2\mathbf{L^3}$ have been determined in two independent and different ways, as follows. Firstly, pure potentiometric titrations have been recorded, from which 5, 4 and 3 protonation constants have been accurately determined for $H_6\mathbf{L^1}$, $H_4\mathbf{L^2}$ and for the model ligand $H_2\mathbf{L^3}$, respectively (Table 1, data in black and Figures S24-S26). A titration combining UV-visible absorption spectrophotometry and potentiometry was then used to confirm some of the log K_H values (Table 1, data in blue) and to characterize the protonated species by means of their electronic spectrum.

Using potentiometric titrations, five of the twelve existing protonation constants could be determined for $\mathbf{L^1}$, while only four (over ten) and three (over six) log K_H could be calculated for $\mathbf{L^2}$ and $\mathbf{L^3}$, respectively. For all three ligands, the most acidic protons (log K_{H5} = 3.21(1), log K_{H4} = 2.81(6) and log K_{H3} = 2.8(1), for $\mathbf{L^1}$, $\mathbf{L^2}$ and $\mathbf{L^3}$, respectively) were attributed to one of the two carboxylate units of the bispidine scaffold. For the model ligand $\mathbf{L^3}$, the protonation constant of the second carboxylate unit of the bispidine scaffold could be also determined (log K_{H2} = 3.42(9)). This comparison with the model ligand $H_2\mathbf{L^3}$ thus suggests that the values of the protonation of the second bispidine carboxylate unit are most likely below 2 for $\mathbf{L^1}$ and $\mathbf{L^2}$ and are not accessible under our experimental conditions. This is also in agreement with the acido-basic properties reported for ligands $\mathbf{L^4}$ and $\mathbf{L^5}$ (Table 1). For $\mathbf{L^1}$, the log K_{H4} (5.02(9)) and log K_{H3} (7.14(7)) values were assigned to the second protonation of $-PO_3^{2-}$ units while the two last most basic log K_H values (log K_{H2} = 9.18(1) and log K_{H1} = 10.62(7)) were attributed to the two tertiary amines of the macrobicyclic bispidine. For $\mathbf{L^2}$, a very different protonation scheme of the tertiary amines of the bispidine skeleton is observed. Indeed, only one protonation constant (log K_{H1} = 10.63(3)) could be determined, as a result of the chair-chair conformation of the bispidine and the stabilization of the ammonium proton inside the cavity by strong *pseudo*-hydrogen bonds with N3, N7 and the pyridyl rings.[31] The highest value measured for $\mathbf{L^2}$ is consistent with the other values previously reported for bispidol ligands such as $\mathbf{L^4}$ (log K_{H1} = 9.54(4))[32] and $\mathbf{L^5}$ (log K_{H1} = 11.15(1))[30] which both adopt a chair-chair conformation[32,30,60,33] as well as with the log K_{H1} = 12.06(6) value measured for the model ligand $\mathbf{L^3}$. On the contrary, two basic protonation constants (log K_{H1} = 10.62(7) and log K_{H2} = 9.18(1)) were determined for the two tertiary amines N7 and N3, respectively. Such protonation scheme has already been reported in rare examples and is most likely associated with a boat-chair or chair-boat conformation more suitable to minimize the electrostatic repulsions between the two positively charged ammoniums.[61,30] One very recent example is ligand $\mathbf{L^6}$ for which comparable protonation constants have been measured and the boat-chair conformation was confirmed by 2D NMR experiments.[40] When $\mathbf{L^1}$, $\mathbf{L^2}$ and **Bispa** ligands are compared, it is very interesting to notice that subtle alterations (carboxylate *versus* ester for **Bispa** and $\mathbf{L^2}$ or pyridine-phosphonate for $\mathbf{L^1}$ *versus* picolinate for $\mathbf{L^2}$) have a marked impact on the ligand conformations and consequently on the protonation patterns. Last, whatever the ligand considered, the other log K_H values that could not be determined under our experimental conditions were assumed to be <2 and are likely related to N-pyridines, and the first protonation of a HPO_3^{2-} function or the remaining carboxylate units.

Table 1. Ligand protonation constants (I = 0.1 M NaCl, 298 K) depending on the conformation of the bispidine ring. Values in parenthesis correspond to 1σ (σ = standard deviation). Data from potentiometric titration are in black; data from UV-visible absorption *versus* pH titration are in blue.

	boat-chair		*chair-chair*				
	L[1][a]	**L**[6] [40]	**L**[2][b]	**L**[3]	**H$_2$bispa**[2] [56]	**L**[4] [32]	**L**[5] [30]
log K_{H_1}	10.62(7)	9.91	10.2(2) 10.54(7)	12.06(6) -	7.45 -	9.54 -	11.15 -
log K_{H_2}	9.18(1) 9.30(2)	9.05 -	6.4(1) 6.53(7)	3.42(9) 3.5(1)	5.62 -	5.11 -	7.35 -
log K_{H_3}	7.14(7)	5.66	3.4(1) 3.3(1)	2.8(1) -	3.31 -	2.99 -	3.78 -
log K_{H_4}	5.02(9) 4.82(3)	3.73 -	2.81(6) -	-	< 2	< 2	3.02
log K_{H_5}	3.21(1)	2.74	< 2	-	< 2	< 2	< 2
log K_{H_6}	< 2	1.40	< 2	-	< 2	< 2	< 2
Σlog K_{H_i}	35.19	32.49	22.83	18.28	16.38	17.64	25.26

[a] For **L**[1], log K_{H6} to log K_{H12} (protonation of the N-pyridine units and second protonation of the phosphonate moieties) could not be determined and were estimated to be below 2. [a] For **L**[2], log K_{H6} to log K_{H10} (protonation of the N-pyridine units and protonation of the second carboxylate of the bispidine scaffold) could not be determined and were estimated to be below 2.

In the case of **L**[1], the determination of the protonated species has also been evaluated by monitoring the variations of the ^{1}H and ^{31}P NMR chemical shifts as a function of pD (Figure 4 for ^{31}P NMR spectra, Figure S27 for ^{1}H NMR spectra).

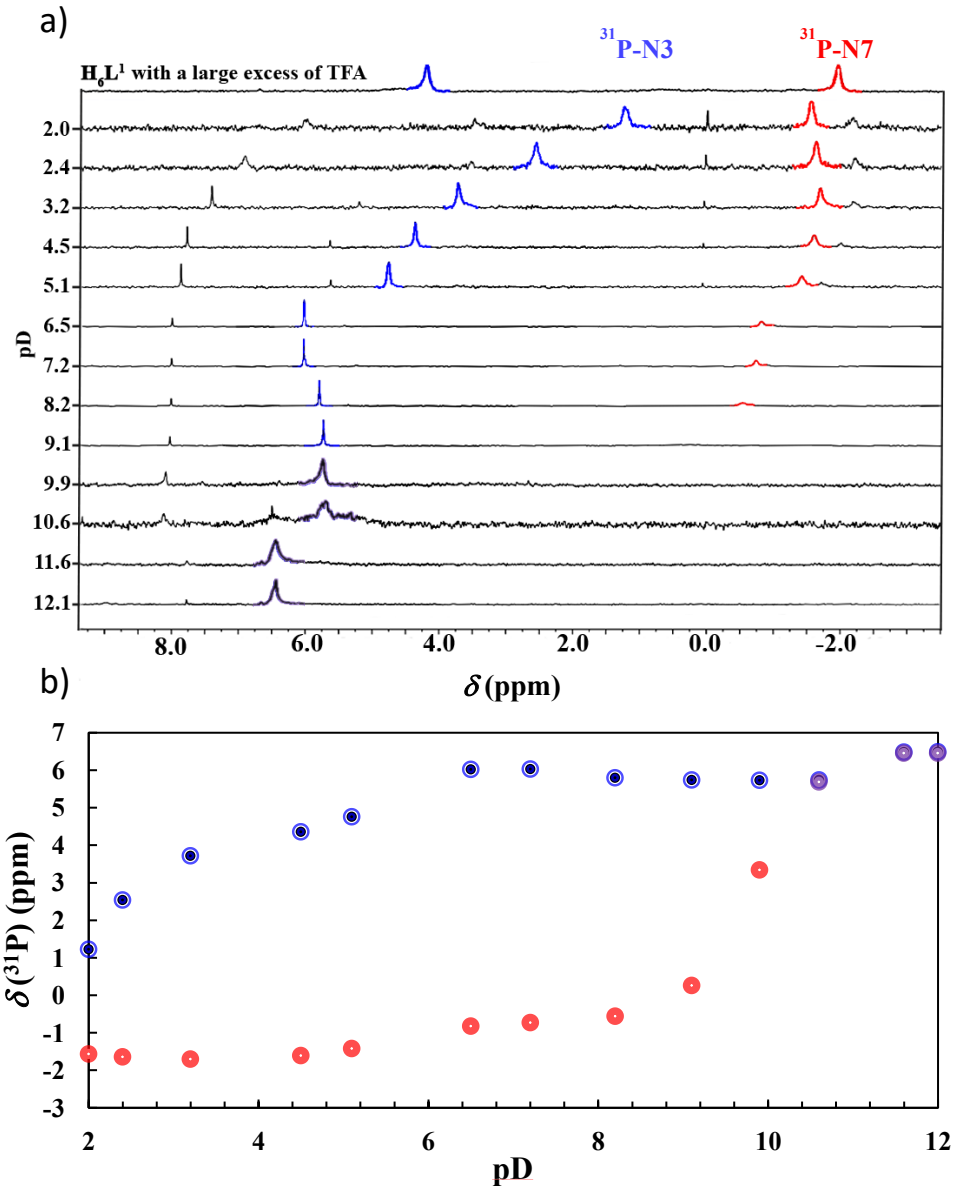

Figure 3. a) ^{31}P NMR spectra (202 MHz, D_2O) of ligand $\mathbf{L^1}$ and its protonated forms as a function of pD ([$\mathbf{L^1}$] = 19.2 mM). b) Variations of the chemical shift of the phosphorus atoms of ligand $\mathbf{L^1}$ as a function of pD. Coalescence of the blue (^{31}P at N3) and red (^{31}P at N7) signals is represented in purple.

First of all, the ^{31}P NMR spectrum in strongly acidic medium (Figure 1a – D_2O + TFA) shows a single set of two peaks at δ_P = 4.12 ppm and δ_P = -2.11 ppm with equivalent integration, which have been unambiguously assigned to the pyridine-phosphonates at N3 and N7, respectively. At pD = 12.1, these two peaks coalesce into a single broad peak centred around δ_P = 6.45 pm (Figure 3a). From pD = 12.1 to 8.2, this main peak splits progressively and one of the new signals undergoes a significant chemical shift during the acidification of the environment

(Figure 3b). This downfield shift is likely related to the protonation of the N7-tertiary amine. It was assumed that, at acidic pH values, the formation of a hydrogen bond between the ammonium and the pyridine-phosphonate substituent places the ^{31}P phosphonate group at N7 in the pyridine shielding cones. A rough estimate of the log K_H value (~ 9.8) could be obtained from the variation of δ_P that is in good agreement with the protonation constants measured by potentiometry (log K_{H1} = 9.18(1)). It is important to note that the protonation at N3 has a negligible influence on the ^{31}P chemical shift, as the pyridine phosphonate substituent is oriented outward from the cavity, as a result from the boat-chair conformation of the bispidine. Minor changes on the δ(^{31}P) of the substituent at N7 can be also seen between pD = 5 and pD = 7, from which a value of log K_H ~ 5.6 could be estimated for the protonation of a -PO_3^{2-} unit (to be compared to log K_{H4} = 5.02(9), Table 1). On a similar manner, significant variations in the chemical shift of the ^{31}P of the substituent at N3 are observed below pD 6.5, which are ascribed to the protonation of the -PO_3^{2-} group of the pyridine phosphonate at N3. Finally, changes are also seen in very acidic conditions due to the protonation of the pyridyl and of the –PO_3H^- groups (log K_H < 2). Formation of minor species (~ 10%) can also be observed between pD = 2 and 12, which tend to disappear under strongly acidic (TFA) or basic conditions, and which could be ascribed to supramolecular arrangements of protonated forms.[62]

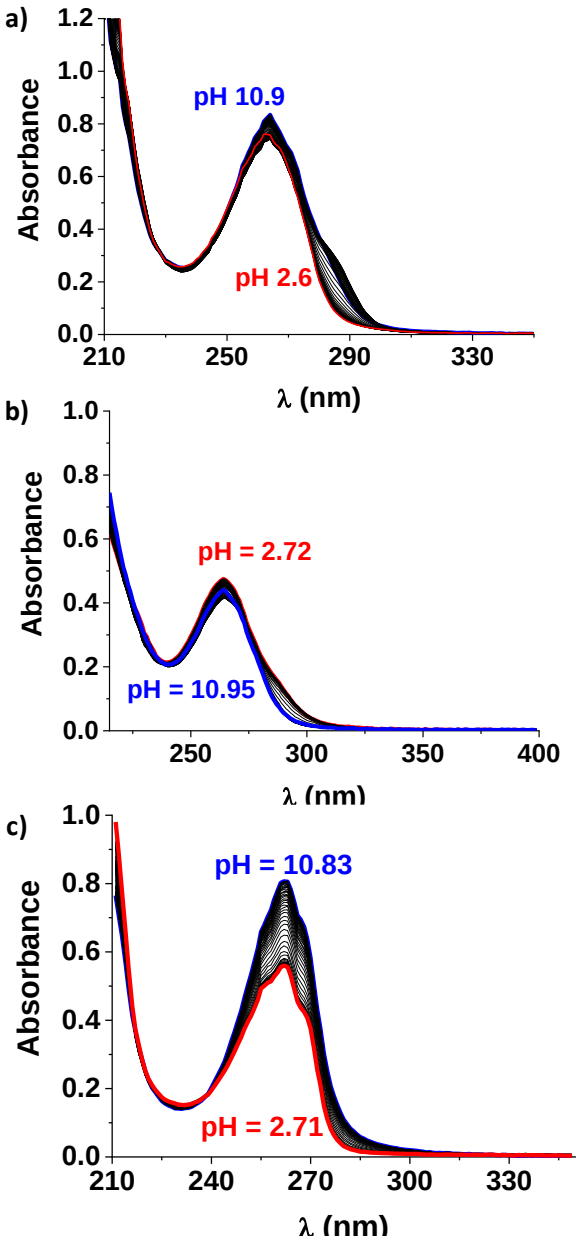

Figure 4. a) UV-Vis absorption spectra *vs* pH titration of ligand L^1 ([$NaCl_{aq}$] = 0.1 M, T = 25°C, c_{ligand} = 5.0 × 10^{-5} M, [$NaOH_{aq}$] = 0.107 mM); b) of ligand L^2 ([$NaCl_{aq}$] = 0.1 M, T = 25°C, c_{ligand} = 3.55 × 10^{-5} M, [$NaOH_{aq}$] = 0.107 mM); c) of ligand **L**^{3} ([$NaCl_{aq}$] = 0.1 M; *T* = 25°C, c_{ligand} = 1.12 × 10^{-4} M, [$NaOH_{aq}$] = 0.107 mM).

For a more detailed assignment of the protonation sites and steps, we then performed UV-visible absorption *versus* pH titrations of ligands **L**^{1}, **L**^{2} and **L**^{3}. Changes of the π-π* transitions centred at about 260-270 nm in the UV-visible absorption spectra were examined as a function of the pH of the solution (Figures 4a and S29 for **L**^{1}, Figures 4b and S31 for **L**^{2} and Figures 4e and S33 for **L**^{3}). These transitions are unambiguously related to the pyridine units which

represent the main chromophores of these bispidine-type ligands and any alteration in these chromophores or in their direct environment are likely to alter their absorption properties. The variations of characteristic absorbance at *ca.* 260 nm as a function of pH and their correlation with the distribution diagrams of the protonated species of ligands $\mathbf{L^3}$, $\mathbf{L^2}$ and $\mathbf{L^1}$ are presented in Figures 4-6. For $\mathbf{L^3}$, a large hypochromic shift was observed from pH 3 to pH 5.5 (Figure 5). The calculated protonation constant (log K_{H2} = 3.5(1)) agrees very well with the value assigned to the carboxylate unit by potentiometric means (log K_{H2} = 3.42(9)). This clearly indicates that this carboxylic unit interacts with the two pyridyl units due to the chair-chair conformation. In the case of $\mathbf{L^2}$, a weak hypochromic shift is first observed under acidic conditions (3 < pH < 5, Figure 6), followed by a much larger hypochromic shift along with the formation of a shoulder at about 285 nm under weakly acidic to neutral conditions (pH 6 to 8). These observations are consistent with successive deprotonation of each of the picolinate units as evidenced by good agreement of the data measured by spectrophotometric *versus* pH titrations (log K_{H3} = 3.3(1) and log K_{H2} = 6.53(7)) and potentiometric titrations (log K_{H3} = 3.4(1) and log K_{H2} = 6.4(1)). Similarly to $\mathbf{L^3}$, absorption variations (hyperchromic shift of the main absorption band) are observed above pH = 9, which is consistent with the deprotonation of the quaternary ammonium with a log K_{H1} = 10.54(7), in agreement with the thermodynamic data extracted from pH-metric measurement (Table 1). As for $\mathbf{L^1}$, a hypochromic shift is seen between pH 7 and pH 9 which can also be ascribed to the deprotonation of one of the two quaternary ammonium sites (log K_{H2} = 9.30(2)). The deprotonation of the quaternary ammonium group in the boat conformation has minimal effect on the pyridyl chromophores and, consequently, does not significantly affect the absorption spectra. Therefore, the corresponding pK_a value of the quaternary ammonium group could not be determined by absorption spectrophotometric titration. It is therefore surmised that the observed protonation constant (log K_{H2} = 9.30(2)) refers to the tertiary amine at N7, which is in chair conformation and can thus interact with the pyridyl chromophores at C2 and C4. This assumption is in perfect agreement with the assignment obtained by ^{31}P NMR pD-titration. Under more acidic conditions, slight absorption changes can be observed in agreement with the deprotonation (log K_{H4} = 4.82(3)) of only one of the two phosphonate groups. The specific conformation of $\mathbf{L^1}$, as revealed by NMR techniques, distinctly impacts the spectrophotometric signatures of each protonated species. This makes it a valuable probe for evaluating the conformation in solution. $\mathbf{L^1}$ most likely adopts a boat-chair conformation as the result of the phosphonate substitutions and to prevent the electrostatic repulsions not only between the two positively charged ammoniums, but mainly between the phosphonate units with double

negative charge. For $\mathbf{L}^2$ bearing mono-charged picolinate units, these electrostatic repulsions are by far much weaker and enable the formation of a chair-chair like conformation.

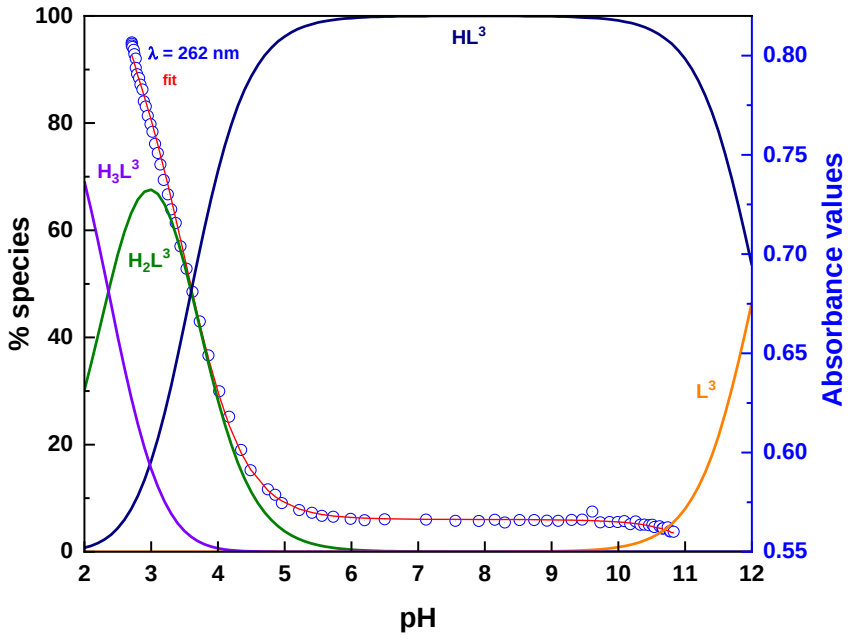

Figure 5. Variation of the absorbance of $\mathbf{L}^3$ at 262 nm as a function of pH and distribution diagram of the protonated species of $\mathbf{L}^3$ (NaCl I = 0.1 M, [$\mathbf{L}^3$] = 1.64 mM). Experimental points ○ and fit –. The distribution diagrams of the protonated species have been calculated according to the log K_H values determined by potentiometric titrations.

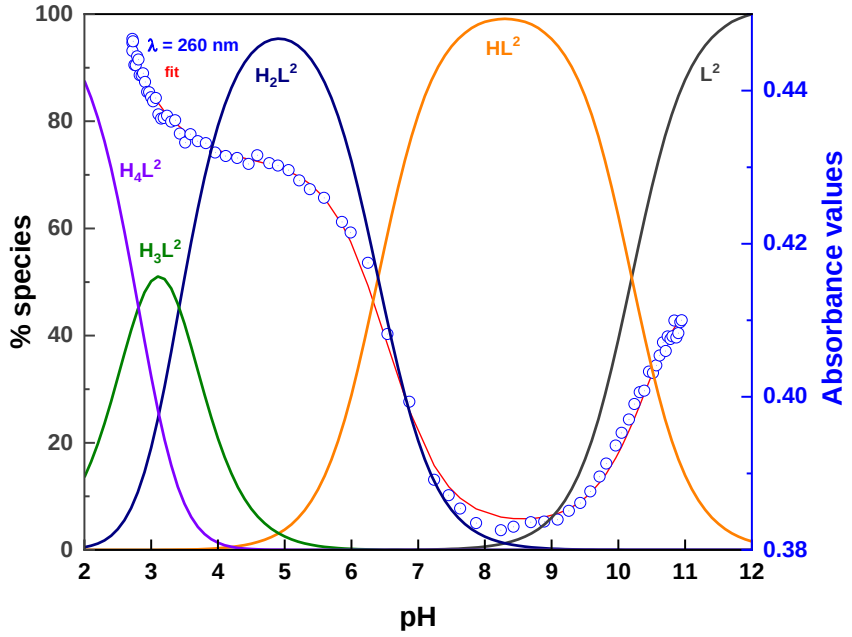

Figure 6. Variation of the absorbance of $\mathbf{L}^2$ at 260 nm as a function of pH and distribution diagram of the protonated species of $\mathbf{L}^2$ (NaCl I = 0.1 M, [$\mathbf{L}^2$] = 1.06 mM). Experimental points

○ and fit –. The distribution diagrams of the protonated species have been calculated according to the log K_H values determined by potentiometric titrations.

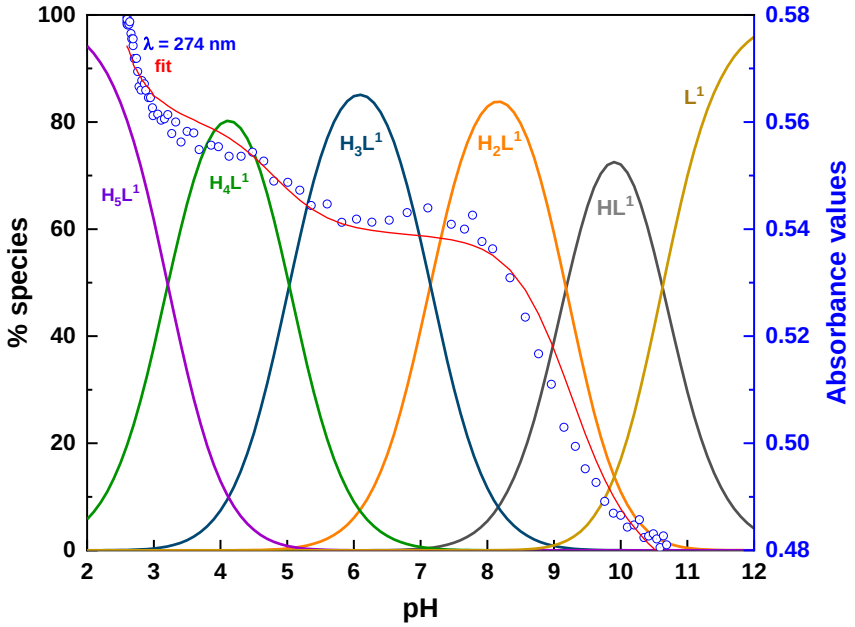

Figure 7. Variation of the absorbance of $\mathbf{L^1}$ at 274 nm as a function of pH and distribution diagram of the protonated species of $\mathbf{L^1}$ (NaCl I = 0.1 M, [$\mathbf{L^1}$] = 1.07 mM). Experimental points ○ and fit –. The distribution diagrams of the protonated species have been calculated according to the log K_H values determined by potentiometric titrations.

Thermodynamic Stability Studies of the Tb(III) Complexes

The thermodynamic stability of the Tb(III) complexes was evaluated by direct potentiometric titrations of solutions of 1:1 stoichiometric mixtures of Tb(III) and ligands. Whatever the ligand considered, only monometallic Tb(III) chelates were evidenced by using 1:1 Tb:L stoichiometric conditions (Table 1, see Figures S34-S35 for titration curves). Very interestingly and in line with the acido-basic properties, the nature of the conformation has a deep impact on the Tb(III) speciation behavior. For $\mathbf{L^2}$ displaying a chair-chair conformation, highly preorganized for metal complexation, only two protonated Tb(III) species were identified and quantified, namely a $[Tb\mathbf{L^2}]^-$ (log K_{TbL2} = 9.7(1)) and a hydroxo species $[Tb(OH)\mathbf{L^2}]^{2-}$ (log $K_{Tb(OH)L2}$ = -10.9(1)). These constants are in good agreement with the data reported for the **Bispa** complexes (Table 2). The observed distribution of species clearly demonstrates that all donor atoms are involved in the Tb(III) coordination (CN = 8, 2 tertiary amines, 2 N-pyridines, 2 bidentate picolinates) and are not protonated within the pH range of 2.5 to 11.5. The coordination sphere of the Tb(III) cation is most likely completed by a water molecule as

suggested by the presence of a hydroxo species at high pH values (> 11.4). Hydroxo complex formation in this pH-range was also observed with the picolinate-based ligand *CHX*OCTAPA.[63] The importance of pre-organization and adequate conformation is highlighted by the thermodynamic data gathered with the $\mathbf{L^1}$ ligand, which reveals, in addition to the presence of a $[TbL^1]^{3-}$ complex (log K_{TbL1} = 9.7(1)), the formation of several protonated species ($[TbHL^1]^{2-}$ with log K_{TbHL1} = 9.87(6), $[TbH_2L^1]^{-}$ with log K_{TbH2L1} = 6.66(3) and $[TbH_3L^1]$ with log K_{TbH3L1} = 3.75(1)) suggesting the absence or a weak participation in the coordination processes of some donors which are then prone to protonation reactions. These protonation sites are most likely related to a phosphonate group and a carboxylate unit. In addition, no hydroxo species were evidenced with $\mathbf{L^1}$.

Table 2. Stability constants of TbL complexes with $\mathbf{L^1}$ and $\mathbf{L^2}$ and pTb values (I = 0.1 M NaCl; 298 K). Values in parenthesis correspond to 1σ (σ = standard deviation). Data from pure potentiometric titration are in black; data from batch titrations by spectrofluorimetry are in green; data from batch titrations by UV-vis absorption spectrophotometry are in blue.

	L^1 (Ln = Tb)	**L^2 (Ln = Tb)**	**Bispa (Ln = La)**	**Bispa (Ln = Lu)**[b]
log K_{LnL}	9.52(6)	9.7(1)	11.42	8.51
log K_{cond} (pH =5.5)	5.4(1) 5.3(2)	4.8(5) 5.1(5)	-	-
log K_{LnHL}	9.87(6)	-	4.07	4.09
log K_{LnH_2L}	6.66(3)	-	-	3.75
log K_{LnH_3L}	3.75(1)	-	-	-
log $K_{Ln(OH)L}$	-	-10.9(1)	-10.92	-
pLn[a]	7.74	7.83	12.0	9.1

[a] pTb calculated for $[Tb(III)]_{tot} = 10^{-6}$ M and $[L]_{tot} = 10^{-5}$ M at pH 7.4. [b] log K values recalculated from ref 56.

These thermodynamic values have been then compared with conditional thermodynamic stability constants recorded at pH 5.5, obtained from batch titrations of ligand solutions at fixed pH by adding aliquots of $TbCl_3$. The pH value of 5.5 was chosen in order to destabilize the Tb(III) complexes sufficiently and to allow an accurate evaluation of the corresponding stability constants. These samples were simultaneously monitored by UV-visible absorption spectrophotometry and spectrofluorimetry. Conditional stability constants were obtained from the statistical processing (non-linear regression program[46,47,48]) of the UV-visible absorption and emission data. The corresponding conditional values are log K_{app} = 5.3(2) (absorption) and log K_{app} = 5.4(1) (emission) for TbL^1 and log K_{app} = 5.1(5) (absorption) and log K_{app} = 4.8(5)

(emission) for Tb$\mathbf{L}^2$ (Figure 8 for $\mathbf{L}^1$ and Figure S36 for $\mathbf{L}^2$). These values are in reasonably good agreement with the conditional stability constants calculated from the thermodynamic stability constants (Table 1) under the same conditions of pH (log K_{cond} = 4.60 with $\mathbf{L}^1$ and log K_{cond} = 4.09 with $\mathbf{L}^2$).

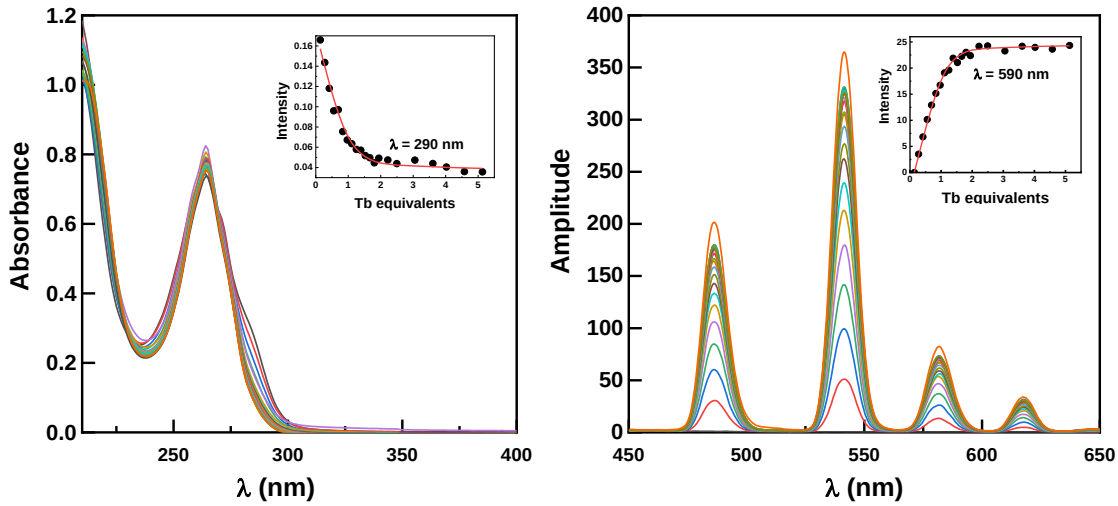

Figure 8. UV-visible absorption spectra (*left*) and luminescence spectra (*right*) of a 50 µM solution of $\mathbf{L}^1$ titrated by increasing amounts of $TbCl_3$ in water (buffer pH 5.5, λ_{ex} = 268 nm). *Insets:* Evolution of the absorbance at 290 nm and of the emission at 590 nm as a function of the equivalents of $TbCl_3$ added and corresponding fit.

The species distribution diagrams as a function of pH (for 1 mM of Tb(**L**), **L** = $\mathbf{L}^1$ or $\mathbf{L}^2$), determined by using the stability and protonation constants from Table 2, are given in Figure 9. In the case of $\mathbf{L}^1$, it was verified that this distribution aligns well with the increase in Tb(III) emission intensity recorded for stoichiometric Tb:$\mathbf{L}^1$ solutions as a function of pH (Figure S37).

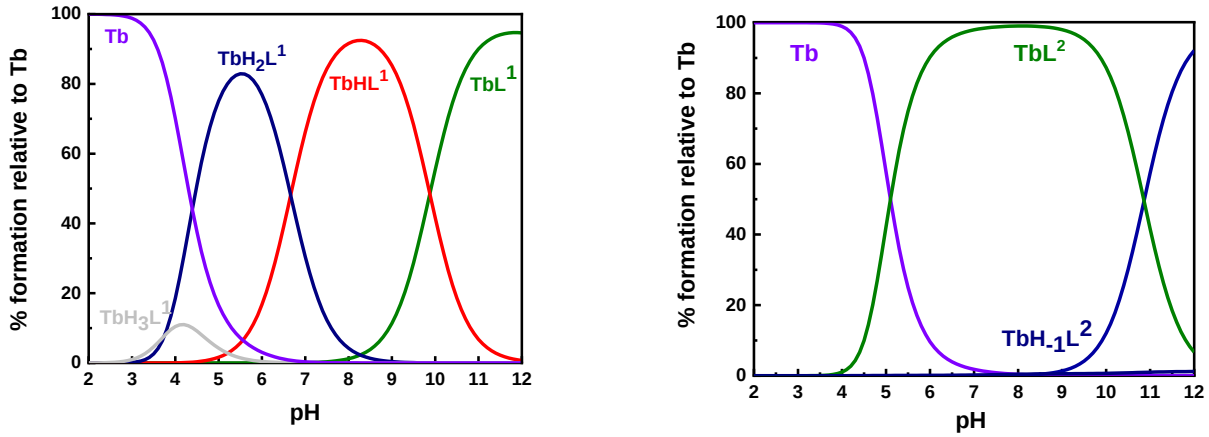

Figure 9. Species distribution diagrams calculated for Tb(III):$\mathbf{L}^1$ (*left*) and Tb(III):$\mathbf{L}^2$ (*right*) ([Tb(III)] = [L] = 1 mM; L = $\mathbf{L}^1$ or $\mathbf{L}^2$).

As shown by the species distribution diagrams, relatively strong thermodynamic stabilities were obtained for Tb**L**^{1} and Tb**L**^{2} allowing the formation of Tb(III) complexes over a wide pH range (pH >3-4) for mM ligand and Tb(III) concentrations. These thermodynamic stability constants are suitable for radiolabeling applications. For instance, calculations indicate that less than 10% of free Tb(III) ions would be present at nanomolar concentrations and in presence of a 1000-fold excess of ligand. In addition, the thermodynamic stability constants (log K_{TbL} = 9.52(6) and 9.7(1) for [Tb**L**^{1}]$^{-}$ and [Tb**L**^{2}]$^{3-}$, respectively) and pTb values (pTb = 7.7 and 7.8 for Tb**L**^{1} and Tb**L**^{2}, respectively) are close to the values previously reported with bispidine-type **Bispa** ligands (Table 2)[56] but they remain far below cyclen-based derivatives[64,65] or other polyazamacrocyclic lanthanide complexes.[64,66-69,28,21] As a comparison, [Gd(DOTA)(H$_2$O)]$^{-}$ displays a thermodynamic stability constant as high as log K_{GdL} = 24.7 and pGd = 18.9,[65] but with the disadvantage of a much slower complexation kinetics. This point is however crucial for an application to biomedical imaging, especially while involving radiolabeling and heat-sensitive biomolecules.

Luminescence properties and kinetic inertness

As stated in the introduction, the kinetic inertness of a metal complex, together with a good thermodynamic stability, is a critical parameter to control when aiming at a biomedical application, especially in the field of medical diagnostics and radiotherapy. To investigate the kinetic inertness of the Tb**L**^{1} and Tb**L**^{2} complexes, we exploited the intense emission of the 4*f*-4*f* transitions of lanthanides ions, specifically the $^{5}D_4 \rightarrow {}^{7}F_J$ (J = 6-3) transitions of Tb(III). For that purpose, the spectroscopic properties of the isolated Tb(III) complexes were thoroughly characterized in water and D$_2$O at pH 7. The corresponding absorption and emission spectra are presented in Figure 10 and additional parameters are presented in Table 3.

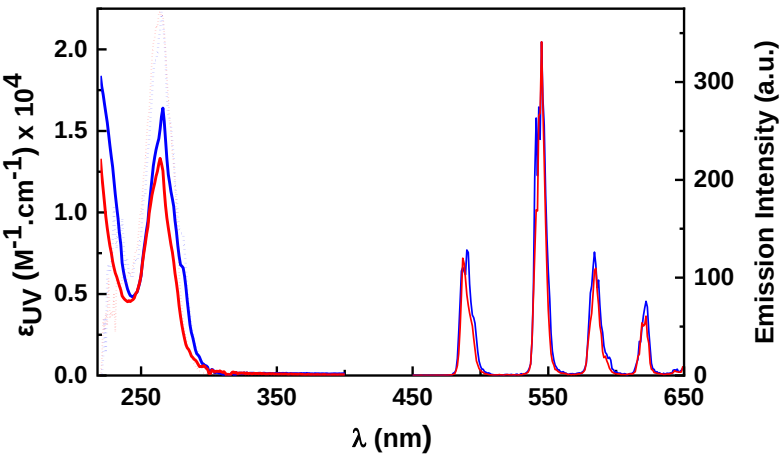

Figure 10. Normalized excitation (dotted lines, λ_{em}= 545 nm), UV-visible absorption (thick straight lines) and normalized emission spectra (λ_{exc}= 263 nm) of a D_2O solution of **TbL^1** (red) and **TbL^2** (blue) at pD = 7.0.

Table 3. Main photophysical parameters of the **TbL^1** and **TbL^2** complexes recorded in water and D_2O at pH = 7.0.

	λ_{exc}	ε_{H_2O} (M^{-1} cm^{-1})	ϕ_{H_2O}[a]	ϕ_{D_2O}[a]	τ_{H_2O} (ms)	τ_{D_2O} (ms)	q[b]
TbL^1	263	13 562	0.15(3)	0.29(6)	1.9(2)	3.3(3)	0.8(2)
TbL^2	263	13 916	0.5(1)	0.6(1)	1.7(2)	2.9(3)	0.9(2)
Tb(bispa)[c]	260	-	-	-	0.95	1.17	0.7(2)
TbL^7[d]	261	16 000	0.68	-	1.95	2.21	0.0(2)

[a] ϕ measured relative to [TbL(H_2O)].[51] [c] Calculated according to reference 52. [c] From reference 34 (pH was not specified). [d] From reference 35.

As expected from previous reports on **bispa** complexes and its analogue **TbL^7**,[34,35] both ligands efficiently sensitize Tb(III) luminescence upon excitation in the π-π* transition of the ligand at 263 nm. For **L^1** or **L^2**, mono-exponential luminescence decays indicate the presence of a unique coordination environment for Tb(III). The determination of the hydration number using the equation defined by Beeby and co-workers[21] confirms the formation of mono-hydrated complexes (q ~ 1), which is in excellent agreement with the physico-chemical approach. In addition, despite the presence of one inner-sphere water molecule, the quantum yield (Φ_{H_2O} = 0.5(1)) and lifetime (τ_{H_2O} = 1.7(2) ms) of **TbL^2** are rather high, in line with data reported for other ligands displaying picolinate antennae effect.[68,70,71] On the other hand, the quantum yield measured for **TbL^1** (Φ_{H_2O} = 0.15(3)) is rather modest despite slightly longer luminescence lifetimes in aqueous solutions (τ_{D_2O} = 3.3(3) ms and τ_{H_2O} = 1.9(2) ms), which might be due to a less efficient sensitization of the $^5D_4$ excited state of Tb(III) by the pyridyl phosphonate antenna.[72,38] The hypothesis of back energy-transfer can be excluded on the basis of the long luminescence lifetimes measured.

Sensitized Tb(III) emission was used to monitor the kinetic inertness of the **TbL^1** and **TbL^2** complexes in various media over a period of two months (Figures 10-11 and Figures S38-S39). In order to mimic transmetalation reactions that may occur in biological media, we followed the transmetalation reaction in the presence of 50 equivalents of Zn(II).[73] At pH = 7.4, **TbL^2** did not show any significant changes in emission intensity over the 2 months of monitoring, regardless of the presence or absence of Zn(II). Good stability was also observed in mouse serum, showing only 12% of decomplexation over 1.6 months. For comparison, the ^{177}Lu

radiolabeled complex with the ligand **bispa**[36] led to 31% decomplexation over 7 days. The proton-assisted decomplexation of **TbL²** was also assessed under acidic conditions (pH = 2), showing much faster decomplexation with a half-life $t_{1/2}$ of 15 days in the absence of Zn(II) (Figure 12) and $t_{1/2}$ of 16 days in the presence of a 50-fold excess of Zn(II) (Figure 12).

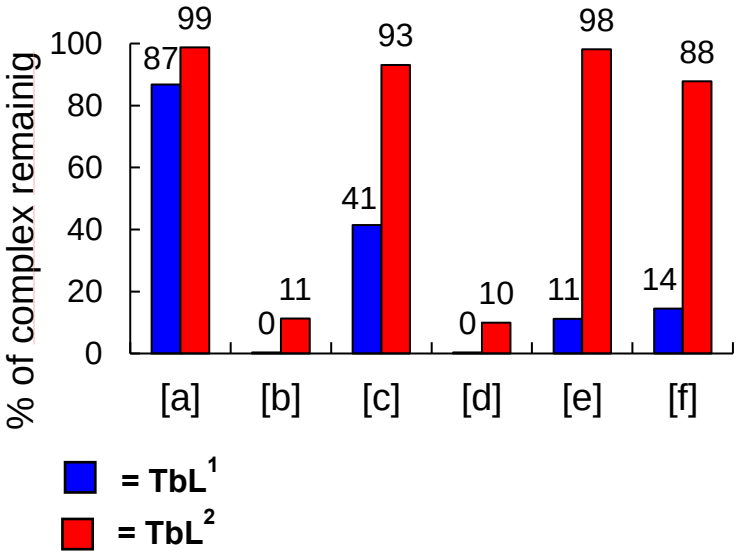

Figure 11. Evolution of the emission intensity of 30 µM solutions of isolated **TbL¹** and **TbL²** over a period of 49 days under various experimental conditions. [a] H_2O at pH = 7.4, [b] H_2O at pH =2.0, [c] 50-fold excess of Zn(II) in H_2O at pH = 7.4, [d] 50-fold excess of Zn(II) in H_2O at pH = 2.0, [e] PBS at pH = 7.4 (137 mM NaCl, 2.7 mM KCl, 10 mM Na_2HPO_4, 1.8 mM KH_2PO_4), and [f] in mouse serum. All solutions were kept at 37°C.

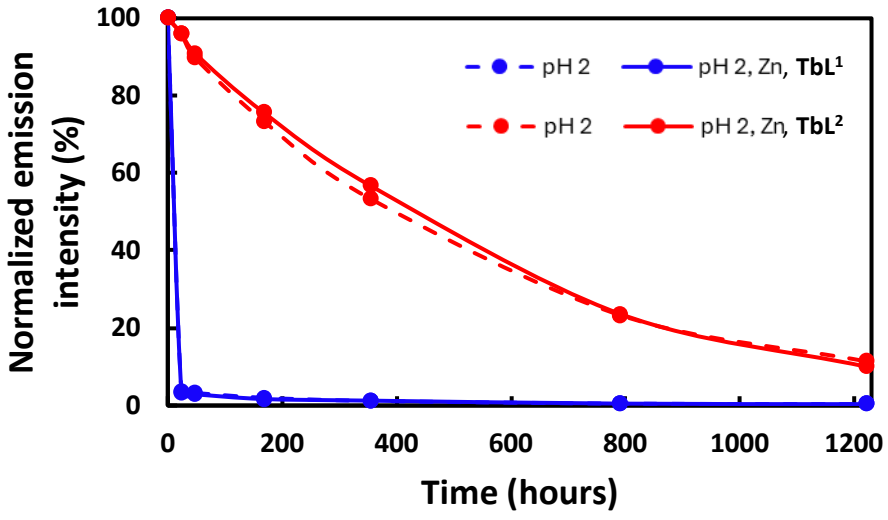

Figure 12. Evolution of the emission intensity of 10 μM solution of isolated **TbL^1** (blue) and **TbL^2** (red) as a function of time under various experimental conditions and determination of the $t_{1/2}$ (H_2O at pH =2.0, dotted lines and 50-fold excess of Zn(II) in H_2O at pH = 2.0, full lines). All solutions were kept at 37°C.

The **TbL^2** complex was also very stable in neutral water, showing only 13% variation of its luminescence intensity over 1.6 months. However, **TbL^1** was significantly less inert under strongly acidic conditions than **TbL^2**, exhibiting a substantial decrease in luminescence intensity over time. From these variations, half-lives of $t_{1/2}$ = 4 h were measured at pH = 2, regardless of the presence of Zn(II). It should be noticed that previous studies on Gd(III) complexes with phosphonate derivatives of DTPA and DOTA have also shown that the higher basicity of the phosphate-bearing ligands tends to favor proton-assisted dissociation. As a figure of comparison, a value of $t_{1/2}$ = 2.5 s was measured for a phosphonate analogue of $[Gd(DTPA)]^{2-}$ (50 μM, 25°C, pH = 4)[74] and a $t_{1/2}$ = 7.9 h (pH = 2, 25°C)[75] was determined for a monophosphonate analogue of $[Gd(DOTA)]^-$, whereas values of the reference complexes amount to 277.8 h and 96 h, for $[Gd(DTPA)]^{2-}$ and $[Gd(DOTA)]^-$, respectively, in similar conditions. The competition with phosphate ions was also monitored at pH = 7.4, using phosphate buffer (PBS, 10 mM Na_2HPO_4, 1.8 mM KH_2PO_4) and, under these conditions, fast decomplexation was also observed with a $t_{1/2}$ of 4h only. The phosphonate complex was also significantly less stable in mouse serum, showing dissociation with a $t_{1/2}$ of 7.8 days, which highlights the strong impact of the ligand substitution on the kinetic inertness of the complex.

Overall, these stability tests reveal that **TbL^1** is significantly less inert than **TbL^2**, which is stable in all media for up to 1.6 months, except at pH = 2, where it remains stable for up to 16 days. Nevertheless, this value remains highly promising for potential *in vivo* applications, especially when compared to the previously measured $t_{1/2}$ = 4 days (pH = 2, 25°C) for $[Gd(DOTA)]^-$.[75] These results are highly significant to validate such bispidine ligands as a potential alternative strategy to prevent lanthanide leaching, nonspecific Tb(III) deposition in tissues and the subsequent development of nephrogenic systemic fibrosis.[76]

Conclusion

We synthesized two bispidine-based octadentate ligands featuring pyridine phosphonate (**L^1**) and picolinate (**L^2**) pendant arms. We demonstrated that the substitution significantly impacted the conformation of the diazabicyclononane skeleton. These conformational variations induced

distinct physicochemical properties, affecting protonation, complexation with Tb(III) ions, as well as the luminescence properties of the resulting complexes. Finally, the kinetic inertness of the two Tb(III) complexes was also evaluated in various model media. Given the rapid complexation kinetics, the good thermodynamic stability, the sizeable luminescent quantum yield (50% in water) and more importantly, its strong kinetic inertness (only 12% decomplexation over 1.6 months of µM solution in mouse serum), **TbL^1** appears to be promising for the further development of lanthanide-based bioimaging probes. Derivatization for future application as a luminescent marker, as well as in nuclear medicine or imaging, by taking advantage of the many Tb radioactive isotopes, holds significant promise.

ASSOCIATED CONTENT

Supporting Information. The following data are available free of charge. ^{1}H and ^{13}C NMR for all ligands and intermediates; ^{31}P NMR of **L^1** ; mass spectra, UV-HPLC chromatograms, ^{1}H-^{1}H COSY, NOESY or ROESY and ^{1}H-^{13}C HSQC spectra for all ligands; potentiometric titration curves for all ligand and Tb complexes with **L^1** and **L^2**; UV-Vis absorption spectra *vs* pH titration of all ligands as well as the electronic absorption spectra of the protonated species involved; UV-visible absorption and luminescence spectra of a **L^2** solution upon titration with $TbCl_3$: pH-dependent variations of Tb(III) emission spectra of 1:1 solution of Tb(III) and **L^1**; kinetic inertness studies of **TbL^1** and **TbL^2**, crystallographic data for compound **1**; all potentiometric titration curves and Hyperquad analysis.

AUTHOR INFORMATION

Corresponding Author

*aline.nonat@unistra.fr, Equipe de Synthèse pour l'Analyse, Université de Strasbourg,

CNRS, IPHC UMR 7178, F-67 037 Strasbourg, France.

Author Contributions

The manuscript was written through contributions of all authors. All authors have given approval to the final version of the manuscript. ‡These authors contributed equally.

Funding Sources

The authors thank the French “Centre National de la Recherche Scientifique” (CNRS), the CNRS MITI founding scheme (PRIME, A. Mahamoud) and the “Fondation Jean-Marie Lehn” (L. Petitpoisson) for founding.

References

(1) Bonnet, C. S.; Tóth, É. Molecular Magnetic Resonance Imaging Probes Based on Ln^{3+} Complexes. In *Advances in Inorganic Chemistry*; van Eldik, R., Hubbard, C. D., Eds.; Insights from Imaging in Bioinorganic Chemistry; Academic Press, **2016**; Vol. 68, pp 43–96. https://doi.org/10.1016/bs.adioch.2015.09.002.

(2) Bünzli, J.-C. G. Benefiting from the Unique Properties of Lanthanide Ions. *Acc. Chem. Res.* **2006**, *39* (1), 53–61. https://doi.org/10.1021/ar0400894.

(3) Chakravarty, R.; Chakraborty, S. A Review of Advances in the Last Decade on Targeted Cancer Therapy Using ^{177}Lu: Focusing on ^{177}Lu Produced by the Direct Neutron Activation Route. *Am. J. Nucl. Med. Mol. Imaging* **2021**, *11* (6), 443–475.

(4) Eliseeva, S. V.; Bünzli, J.-C. G. Lanthanide Luminescence for Functional Materials and Bio-Sciences. *Chem. Soc. Rev.* **2009**, *39* (1), 189–227. https://doi.org/10.1039/B905604C.

(5) Caille, J.; Kien, P.; Allard, M.; Bonnemain, B. A New Contrast Agent for Use in Neuroradiological MRI, Dota Gadolinium. *Am. J. Neuroradiol.* **1986**, *7* (3), 540–540.

(6) Magerstädt, M.; Gansow, O. A.; Brechbiel, M. W.; Colcher, D.; Baltzer, L.; Knop, R. H.; Girton, M. E.; Naegele, M. Gd(DOTA): An Alternative to Gd(DTPA) as a $T_{1,2}$ Relaxation Agent for NMR Imaging or Spectroscopy. *Magn. Reson. Med.* **1986**, *3*, 808–812. https://doi.org/10.1002/mrm.1910030517.

(7) Wahsner, J.; Gale, E. M.; Rodriguez-Rodriguez, A.; Caravan, P. Chemistry of MRI Contrast Agents: Current Challenges and New Frontiers. *Chem. Rev.* **2019**, *119* (2), 957–1057. https://doi.org/10.1021/acs.chemrev.8b00363.

(8) Sy, M.; Nonat, A.; Hildebrandt, N.; Charbonnière, L. J. Lanthanide-Based Luminescence Biolabelling. *Chem. Commun.* **2016**, *52* (29), 5080–5095. https://doi.org/10.1039/C6CC00922K.

(9) Manafi-Farid, R.; Ataeinia, B.; Ranjbar, S.; Jamshidi Araghi, Z.; Moradi, M. M.; Pirich, C.; Beheshti, M. ImmunoPET: Antibody-Based PET Imaging in Solid Tumors. *Front. Med. (Lausanne)* **2022**, *9*, 916693. https://doi.org/10.3389/fmed.2022.916693.

(10) Al-Ibraheem, A.; Scott, A. M. Tb-161-PSMA Unleashed: A Promising New Player in the Theranostics of Prostate Cancer. *Nucl. Med. Molec. Imag.* **2023**, *57*, 168–171. https://doi.org/10.1007/s13139-023-00804-7.

(11) Muller, C.; Behe, M.; Geistlich, S.; van der Meulen, N. P.; Schibli, R. Targeted Radiotherapeutics from “Bench-to-Bedside.” *Chimia* **2020**, *74* (12), 939–945. https://doi.org/10.2533/chimia.2020.939.

(12) Banerjee, S.; Pillai, M. R. A.; Knapp, F. F. (Russ). Lutetium-177 Therapeutic Radiopharmaceuticals: Linking Chemistry, Radiochemistry, and Practical Applications. *Chem. Rev.* **2015**, *115* (8), 2934–2974. https://doi.org/10.1021/cr500171e.

(13) Klaassen, N. J. M.; Arntz, M. J.; Gil Arranja, A.; Roosen, J.; Nijsen, J. F. W. The Various Therapeutic Applications of the Medical Isotope Holmium-166: A Narrative Review. *EJNMMI Radiopharm. Chem.* **2019**, *4* (1), 19. https://doi.org/10.1186/s41181-019-0066-3.

(14) Kazakov, A. G. Terbium Isotopes in Nuclear Medicine: Production, Recovery, and Application. *Radiochemistry* **2022**, *64* (2), 103–119. https://doi.org/10.1134/S1066362222020011.

(15) Mueller, C.; Zhernosekov, K.; Koester, U.; Johnston, K.; Dorrer, H.; Hohn, A.; van der Walt, N. T.; Tuerler, A.; Schibli, R. A Unique Matched Quadruplet of Terbium Radioisotopes for PET and

SPECT and for Alpha- and Beta(-)-Radionuclide Therapy: An In Vivo Proof-of-Concept Study with a New Receptor-Targeted Folate Derivative. *J. Nucl. Med.* **2012**, *53* (12), 1951–1959. https://doi.org/10.2967/jnumed.112.107540.

(16) Borgna, F.; Haller, S.; Rodriguez, J. M. M.; Ginj, M.; Grundler, P.; Zeevaart, J. R.; Koster, U.; Schibli, R.; van der Meulen, N. P.; Mueller, C. Combination of Terbium-161 with Somatostatin Receptor Antagonists-a Potential Paradigm Shift for the Treatment of Neuroendocrine Neoplasms. *Eur. J. Nucl. Med. Mol. Imaging* **2022**, *49* (4), 1113–1126. https://doi.org/10.1007/s00259-021-05564-0.

(17) *Terbium: a new 'Swiss army knife' for nuclear medicine*. CERN Courier. https://cerncourier.com/a/terbium-a-new-swiss-army-knife-for-nuclear-medicine/, **2013**.

(18) Price, E. W.; Orvig, C. Matching Chelators to Radiometals for Radiopharmaceuticals. *Chem. Soc. Rev.* **2013**, *43* (1), 260–290. https://doi.org/10.1039/C3CS60304K.

(19) Boros, E.; Holland, J. P. Chemical Aspects of Metal Ion Chelation in the Synthesis and Application Antibody-Based Radiotracers. *J. Labelled Comp. Radiopharm.* **2018**, *61* (9), 652–671. https://doi.org/10.1002/jlcr.3590.

(20) Simms, M. E.; Li, Z.; Sibley, M. M.; Ivanov, A. S.; Lara, C. M.; Johnstone, T. C.; Kertesz, V.; Fears, A.; White, F. D.; Thorek, D. L. J.; Thiele, N. A. PYTA: A Universal Chelator for Advancing the Theranostic Palette of Nuclear Medicine. *Chem. Sci.* **2024**. https://doi.org/10.1039/D3SC06854D.

(21) Guillou, A.; Galland, M.; Roux, A.; Váradi, B.; Gogolák, R. A.; Le Saëc, P.; Faivre-Chauvet, A.; Beyler, M.; Bucher, C.; Tircsó, G.; Patinec, V.; Maury, O.; Tripier, R. Picolinate-Appended Tacn Complexes for Bimodal Imaging: Radiolabeling, Relaxivity, Photophysical and Electrochemical Studies. *J. Inorg. Biochem.* **2020**, *205*, 110978. https://doi.org/10.1016/j.jinorgbio.2019.110978.

(22) Ferdani, R.; Stigers, D. J.; Fiamengo, A. L.; Wei, L.; Li, B. T. Y.; Golen, J. A.; Rheingold, A. L.; Weisman, G. R.; Wong, E. H.; Anderson, C. J. Synthesis, Cu(II) Complexation, ^{64}Cu-Labeling and Biological Evaluation of Cross-Bridged Cyclam Chelators with Phosphonate Pendant Arms. *Dalton Trans.* **2012**, *41* (7), 1938–1950. https://doi.org/10.1039/C1DT11743B.

(23) David, T.; Hlinová, V.; Kubíček, V.; Bergmann, R.; Striese, F.; Berndt, N.; Szöllősi, D.; Kovács, T.; Máthé, D.; Bachmann, M.; Pietzsch, H.-J.; Hermann, P. Improved Conjugation, 64-Cu Radiolabeling, in Vivo Stability, and Imaging Using Nonprotected Bifunctional Macrocyclic Ligands: Bis(Phosphinate) Cyclam (BPC) Chelators. *J. Med. Chem.* **2018**, *61* (19), 8774–8796. https://doi.org/10.1021/acs.jmedchem.8b00932.

(24) Bodei, L.; Cremonesi, M.; Ferrari, M.; Pacifici, M.; Grana, C. M.; Bartolomei, M.; Baio, S. M.; Sansovini, M.; Paganelli, G. Long-Term Evaluation of Renal Toxicity after Peptide Receptor Radionuclide Therapy with ^{90}Y-DOTATOC and ^{177}Lu-DOTATATE: The Role of Associated Risk Factors. *Eur. J. Nucl. Med. Mol. Imaging* **2008**, *35* (10), 1847–1856. https://doi.org/10.1007/s00259-008-0778-1.

(25) Dai, L.; Jones, C. M.; Chan, W. T. K.; Pham, T. A.; Ling, X.; Gale, E. M.; Rotile, N. J.; Tai, W. C.-S.; Anderson, C. J.; Caravan, P.; Law, G.-L. Chiral DOTA Chelators as an Improved Platform for Biomedical Imaging and Therapy Applications. *Nat. Commun.* **2018**, *9* (1), 857. https://doi.org/10.1038/s41467-018-03315-8.

(26) Wood, J. L.; Ghosh, S.; Houston, Z. H.; Fletcher, N. L.; Humphries, J.; Mardon, K.; Akhter, D. T.; Tieu, W.; Ivashkevich, A.; Wheatcroft, M. P.; Thurecht, K. J.; Codd, R. A First-in-Class Dual-Chelator Theranostic Agent Designed for Use with Imaging-Therapy Radiometal Pairs of Different Elements. *Chem. Sci.* **2024**. https://doi.org/10.1039/D4SC02851A.

(27) Bussi, S.; Coppo, A.; Botteron, C.; Fraimbault, V.; Fanizzi, A.; De Laurentiis, E.; Colombo Serra, S.; Kirchin, M. A.; Tedoldi, F.; Maisano, F. Differences in Gadolinium Retention after Repeated Injections of Macrocyclic MR Contrast Agents to Rats. *J. Magn. Reson. Imaging* **2018**, *47*, 746–752. https://doi.org/10.1002/jmri.25822.

(28) Nizou, G.; Favaretto, C.; Borgna, F.; Grundler, P. V.; Saffon-Merceron, N.; Platas-Iglesias, C.; Fougère, O.; Rousseaux, O.; van der Meulen, N. P.; Müller, C.; Beyler, M.; Tripier, R. Expanding

the Scope of Pyclen-Picolinate Lanthanide Chelates to Potential Theranostic Applications. *Inorg. Chem.* **2020**, *59* (16), 11736–11748. https://doi.org/10.1021/acs.inorgchem.0c01664.
(29) Ndiaye, D.; Sy, M.; Pallier, A.; Même, S.; de Silva, I.; Lacerda, S.; Nonat, A. M.; Charbonnière, L. J.; Tóth, É. Unprecedented Kinetic Inertness for a Mn^{2+} -Bispidine Chelate: A Novel Structural Entry for Mn^{2+} -Based Imaging Agents. *Angew. Chem. Int. Ed. Engl.* **2020**, *59*, 11958–11963. https://doi.org/10.1002/anie.202003685.
(30) Sy, M.; Ndiaye, D.; da Silva, I.; Lacerda, S.; Charbonnière, L. J.; Tóth, É.; Nonat, A. M. $^{55/52}Mn^{2+}$ Complexes with a Bispidine-Phosphonate Ligand: High Kinetic Inertness for Imaging Applications. *Inorg. Chem.* **2022**, *61* (34), 13421–13432. https://doi.org/10.1021/acs.inorgchem.2c01681.
(31) Nonat, A. M.; Roux, A.; Sy, M.; Charbonnière, L. J. 2,4-Substituted Bispidines as Rigid Hosts for Versatile Applications: From κ-Opioid Receptor to Metal Coordination. *Dalton Trans.* **2019**, *48* (44), 16476–16492. https://doi.org/10.1039/C9DT03480C.
(32) Gillet, R.; Roux, A.; Brandel, J.; Huclier-Markai, S.; Camerel, F.; Jeannin, O.; Nonat, A. M.; Charbonnière, L. J. A Bispidol Chelator with a Phosphonate Pendant Arm: Synthesis, Cu(II) Complexation, and ^{64}Cu Labeling. *Inorg. Chem.* **2017**, *56* (19), 11738–11752. https://doi.org/10.1021/acs.inorgchem.7b01731.
(33) Roux, A.; Gillet, R.; Huclier-Markai, S.; Ehret-Sabatier, L.; Charbonnière, L. J.; Nonat, A. M. Bifunctional Bispidine Derivatives for Copper-64 Labelling and Positron Emission Tomography. *Org. Biomol. Chem.* **2017**, *15* (6), 1475–1483. https://doi.org/10.1039/C6OB02712A.
(34) Braun, F.; Comba, P.; Grimm, L.; Herten, D.-P.; Pokrandt, B.; Wadepohl, H. Ligand-Sensitized Lanthanide(III) Luminescence with Octadentate Bispidines. *Inorg. Chim. Acta* **2019**, *484*, 464–468. https://doi.org/10.1016/j.ica.2018.09.078.
(35) Abad-Galán, L.; Cieslik, P.; Comba, P.; Gast, M.; Maury, O.; Neupert, L.; Roux, A.; Wadepohl, H. Excited State Properties of Lanthanide(III) Complexes with a Nonadentate Bispidine Ligand. *Chem. Eur. J.* **2021**, *27*, 10303–10312. https://doi.org/10.1002/chem.202005459.
(36) Cieslik, P.; Kubeil, M.; Zarschler, K.; Ullrich, M.; Brandt, F.; Anger, K.; Wadepohl, H.; Kopka, K.; Bachmann, M.; Pietzsch, J.; Stephan, H.; Comba, P. Toward Personalized Medicine: One Chelator for Imaging and Therapy with Lutetium-177 and Actinium-225. *J. Am. Chem. Soc.* **2022**, *144* (47), 21555–21567. https://doi.org/10.1021/jacs.2c08438.
(37) Kopp, I.; Cieslik, P.; Anger, K.; Josephy, T.; Neupert, L.; Velmurugan, G.; Gast, M.; Wadepohl, H.; Brühlmann, S. A.; Walther, M.; Kopka, K.; Bachmann, M.; Stephan, H.; Kubeil, M.; Comba, P. Bispidine Chelators for Radiopharmaceutical Applications with Lanthanide, Actinide, and Main Group Metal Ions. *Inorg. Chem.* **2023**, *62* (50), 20754–20768. https://doi.org/10.1021/acs.inorgchem.3c02340.
(38) Salaam, J.; Tabti, L.; Bahamyirou, S.; Lecointre, A.; Hernandez Alba, O.; Jeannin, O.; Camerel, F.; Cianférani, S.; Bentouhami, E.; Nonat, A. M.; Charbonnière, L. J. Formation of Mono- and Polynuclear Luminescent Lanthanide Complexes Based on the Coordination of Preorganized Phosphonated Pyridines. *Inorg. Chem.* **2018**, *57* (10), 6095–6106. https://doi.org/10.1021/acs.inorgchem.8b00666.
(39) Hamon, N.; Godec, L.; Jourdain, E.; Lucio-Martínez, F.; Platas-Iglesias, C.; Beyler, M.; Charbonnière, L. J.; Tripier, R. Synthesis and Photophysical Properties of Lanthanide Pyridinylphosphonic Tacn and Pyclen Derivatives: From Mononuclear Complexes to Supramolecular Heteronuclear Assemblies. *Inorg. Chem.* **2023**, *62* (46), 18940–18954. https://doi.org/10.1021/acs.inorgchem.3c02522.
(40) Ndiaye, D.; Sy, M.; Thor, W.; Charbonnière, L. J.; Nonat, A. M.; Tóth, É. Structural Variations in Carboxylated Bispidine Ligands: Influence of Positional Isomerism and Rigidity on the Conformation, Stability, Inertness and Relaxivity of Their Mn^{2+} Complexes. *Chem. Eur. J.* **2023**, *29*, e202301880. https://doi.org/10.1002/chem.202301880.
(41) Gottlieb, H. E.; Kotlyar, V.; Nudelman, A. NMR Chemical Shifts of Common Laboratory Solvents as Trace Impurities. *J. Org. Chem.* **1997**, *62* (21), 7512–7515. https://doi.org/10.1021/jo971176v.

(42) Mikkelsen, K.; Nielsen, S. O. Acidity measurements with the glass electrode in H_2O-D_2O mixtures. *J. Phys. Chem.* **1960**, *64* (5), 632–637. https://doi.org/10.1021/j100834a026.
(43) *Méthodes d'analyse Complexométriques Avec Les Titriplex*; Merck E: Darmstadt, **1990**.
(44) Knighton, R. C.; Troadec, T.; Mazan, V.; Le Saec, P.; Marionneau-Lambot, S.; Le Bihan, T.; Saffon-Merceron, N.; Le Bris, N.; Cherel, M.; Faivre-Chauvet, A.; Elhabiri, M.; Charbonniere, L. J.; Tripier, R. Cyclam-Based Chelators Bearing Phosphonated Pyridine Pendants for ^{64}Cu-PET Imaging: Synthesis, Physicochemical Studies, Radiolabeling, and Bioimaging. *Inorg. Chem.* **2021**, *60* (4), 2634–2648. https://doi.org/10.1021/acs.inorgchem.0c03492.
(45) Gans, P.; Sabatini, A.; Vacca, A. Investigation of Equilibria in Solution. Determination of Equilibrium Constants with the HYPERQUAD Suite of Programs. *Talanta* **1996**, *43* (10), 1739–1753. https://doi.org/10.1016/0039-9140(96)01958-3.
(46) Gampp, H.; Maeder, M.; Meyer, C.; Zuberbuhler, A. Calculation of Equilibrium-Constants from Multiwavelength Spectroscopic Data .1. Mathematical Considerations. *Talanta* **1985**, *32* (2), 95–101. https://doi.org/10.1016/0039-9140(85)80035-7.
(47) Gampp, H.; Maeder, M.; Meyer, C.; Zuberbuhler, A. Calculation of Equilibrium-Constants from Multiwavelength Spectroscopic Data .4. Model-Free Least-Squares Refinement by Use of Evolving Factor-Analysis. *Talanta* **1986**, *33* (12), 943–951. https://doi.org/10.1016/0039-9140(86)80233-8.
(48) Hippler, H. Data Fitting in the Chemical Sciences. P. Gans. Wiley, Chichester, 1992. XII, 258 S. *Angew. Chem.* **1993**, *105*, 654–654. https://doi.org/10.1002/ange.19931050453.
(49) Marquardt, D. W. An Algorithm for Least-Squares Estimation of Nonlinear Parameters. *SIAM* **1963**, *11*, 431–441. https://doi.org/10.1137/0111030.
(50) Characteristics of Fluorescence Emission. In *Molecular Fluorescence*; John Wiley & Sons, Ltd, **2012**; pp 53–74. https://doi.org/10.1002/9783527650002.ch3.
(51) Weibel, N.; Charbonnière, L. J.; Guardigli, M.; Roda, A.; Ziessel, R. Engineering of Highly Luminescent Lanthanide Tags Suitable for Protein Labeling and Time-Resolved Luminescence Imaging. *J. Am. Chem. Soc.* **2004**, *126* (15), 4888–4896. https://doi.org/10.1021/ja031886k.
(52) Beeby, A.; Clarkson, I. M.; Dickins, R. S.; Faulkner, S.; Parker, D.; Royle, L.; de Sousa, A. S.; Williams, J. A. G.; Woods, M. Non-Radiative Deactivation of the Excited States of Europium, Terbium and Ytterbium Complexes by Proximate Energy-Matched OH, NH and CH Oscillators: An Improved Luminescence Method for Establishing Solution Hydration States. *J. Chem. soc., Perkin Trans. 2*. **1999**, pp 493–504.
(53) Altomare, A.; Cascarano, G.; Giacovazzo, C.; Guagliardi, A.; Burla, M. C.; Polidori, G.; Camalli, M. SIR92 – a Program for Automatic Solution of Crystal Structures by Direct Methods. *J. Appl. Cryst.* **1994**, *27* (3), 435–435. https://doi.org/10.1107/S002188989400021X.
(54) Sheldrick, G. M. Crystal Structure Refinement with SHELXL. *Acta Cryst. C* **2015**, *71* (1), 3–8. https://doi.org/10.1107/S2053229614024218.
(55) Farrugia, L. J. WinGX and ORTEP for Windows: An Update. *J. Appl. Cryst.* **2012**, *45* (4), 849–854. https://doi.org/10.1107/S0021889812029111.
(56) Comba, P.; Jermilova, U.; Orvig, C.; Patrick, B. O.; Ramogida, C. F.; Rueck, K.; Schneider, C.; Starke, M. Octadentate Picolinic Acid-Based Bispidine Ligand for Radiometal Ions. *Chem.-Eur. J.* **2017**, *23* (63), 15945–15956. https://doi.org/10.1002/chem.201702284.
(57) Kolanowski, J. L.; Jeanneau, E.; Steinhoff, R.; Hasserodt, J. Bispidine Platform Grants Full Control over Magnetic State of Ferrous Chelates in Water. *Chem. Eur. J.* **2013**, *19* (27), 8839–8849. https://doi.org/10.1002/chem.201300604.
(58) Bruchertseifer, F.; Comba, P.; Martin, B.; Morgenstern, A.; Notni, J.; Starke, M.; Wadepohl, H. First-Generation Bispidine Chelators for $^{213}Bi^{III}$ Radiopharmaceutical Applications. *ChemMedChem* **2020**, *15*, 1591–1600. https://doi.org/10.1002/cmdc.202000361.
(59) Southern, S. A.; Nag, T.; Kumar, V.; Triglav, M.; Levin, K.; Bryce, D. L. NMR Response of the Tetrel Bond Donor. *J. Phys. Chem. C* **2022**, *126* (1), 851–865. https://doi.org/10.1021/acs.jpcc.1c10121.

(60) Roux, A.; Nonat, A. M.; Brandel, J.; Hubscher-Bruder, V.; Charbonnière, L. J. Kinetically Inert Bispidol-Based Cu(II) Chelate for Potential Application to 64/67Cu Nuclear Medicine and Diagnosis. *Inorg. Chem.* **2015**, *54* (9), 4431–4444. https://doi.org/10.1021/acs.inorgchem.5b00207.
(61) Norrehed, S.; Erdélyi, M.; E. Light, M.; Gogoll, A. Protonation-Triggered Conformational Modulation of an N , N ’-Dialkylbispidine: First Observation of the Elusive Boat–Boat Conformer. *Organic & Biomolecular Chemistry* **2013**, *11* (37), 6292–6299. https://doi.org/10.1039/C3OB41122B.
(62) Elhabiri, M.; Abada, S.; Sy, M.; Nonat, A.; Choquet, P.; Esteban-Gómez, D.; Cassino, C.; Platas-Iglesias, C.; Botta, M.; Charbonnière, L. J. Importance of Outer-Sphere and Aggregation Phenomena in the Relaxation Properties of Phosphonated Gadolinium Complexes with Potential Applications as MRI Contrast Agents. *Chem. Eur. J.* **2015**, *21* (17), 6535–6546. https://doi.org/10.1002/chem.201500155.
(63) Lucio-Martínez, F.; Garda, Z.; Váradi, B.; Kálmán, F. K.; Esteban-Gómez, D.; Tóth, É.; Tircsó, G.; Platas-Iglesias, C. Rigidified Derivative of the Non-Macrocyclic Ligand H_4OCTAPA for Stable Lanthanide(III) Complexation. *Inorg. Chem.* **2022**, *61* (12), 5157–5171. https://doi.org/10.1021/acs.inorgchem.2c00501.
(64) Clarke, E. T.; Martell, A. E. Stabilities of Trivalent Metal Ion Complexes of the Tetraacetate Derivatives of 12-, 13- and 14-Membered Tetraazamacrocycles. *Inorg. Chim. Acta* **1991**, *190* (1), 37–46. https://doi.org/10.1016/S0020-1693(00)80229-7.
(65) Cacheris, W. P.; Nickle, S. K.; Sherry, A. D. Thermodynamic Study of Lanthanide Complexes of 1,4,7-Triazacyclononane-N,N’,N"-Triacetic Acid and 1,4,7,10-Tetraazacyclododecane-N,N’,N",N’’’-Tetraacetic Acid. *Inorg. Chem.* **1987**, *26* (6), 958–960. https://doi.org/10.1021/ic00253a038.
(66) Price, E. W.; Cawthray, J. F.; Bailey, G. A.; Ferreira, C. L.; Boros, E.; Adam, M. J.; Orvig, C. H4octapa: An Acyclic Chelator for 111In Radiopharmaceuticals. *J. Am. Chem. Soc.* **2012**, *134* (20), 8670–8683. https://doi.org/10.1021/ja3024725.
(67) Kalman, F. K.; Vegh, A.; Regueiro-Figueroa, M.; Toth, E.; Platas-Iglesias, C.; Tircso, G. H_4Octapa: Highly Stable Complexation of Lanthanide(III) Ions and Copper(II). *Inorg. Chem.* **2015**, *54* (5), 2345–2356. https://doi.org/10.1021/ic502966m.
(68) Le Fur, M.; Molnár, E.; Beyler, M.; Fougère, O.; Esteban-Gómez, D.; Rousseaux, O.; Tripier, R.; Tircsó, G.; Platas-Iglesias, C. Expanding the Family of Pyclen-Based Ligands Bearing Pendant Picolinate Arms for Lanthanide Complexation. *Inorg. Chem.* **2018**, *57* (12), 6932–6945. https://doi.org/10.1021/acs.inorgchem.8b00598.
(69) Leygue, N.; Galaup, C.; Lopera, A.; Delgado-Pinar, E.; Williams, R. M.; Gornitzka, H.; Zwier, J. M.; García-España, E.; Lamarque, L.; Picard, C. Tripyridinophane Platform Containing Three Acetate Pendant Arms: An Attractive Structural Entry for the Development of Neutral Eu(III) and Tb(III) Complexes in Aqueous Solution. *Inorg. Chem.* **2020**, *59* (2), 1496–1512. https://doi.org/10.1021/acs.inorgchem.9b03345.
(70) Nonat, A.; Gateau, C.; Fries, P. H.; Mazzanti, M. Lanthanide Complexes of a Picolinate Ligand Derived from 1,4,7-Triazacyclononane with Potential Application in Magnetic Resonance Imaging and Time-Resolved Luminescence Imaging. *Chem. Eur. J.* **2006**, *12* (27), 7133–7150. https://doi.org/10.1002/chem.200501390.
(71) Regueiro-Figueroa, M.; Bensenane, B.; Ruscsák, E.; Esteban-Gómez, D.; Charbonnière, L. J.; Tircsó, G.; Tóth, I.; de Blas, A.; Rodríguez-Blas, T.; Platas-Iglesias, C. Lanthanide Dota-like Complexes Containing a Picolinate Pendant: Structural Entry for the Design of Ln(III)-Based Luminescent Probes. *Inorg. Chem.* **2011**, *50* (9), 4125–4141. https://doi.org/10.1021/ic2001915.
(72) Charpentier, C.; Salaam, J.; Lecointre, A.; Jeannin, O.; Nonat, A.; Charbonnière, L. J. Phosphonated Podand Type Ligand for the Complexation of Lanthanide Cations Phosphonated Podand Type Ligand for the Complexation of Lanthanide Cations. **2019**, *2019* (16), 2168–2174. https://doi.org/10.1002/ejic.201900069.

(73) Gale, E. M.; Atanasova, I. P.; Blasi, F.; Ay, I.; Caravan, P. A Manganese Alternative to Gadolinium for MRI Contrast. *J. Am. Chem. Soc.* **2015**, *137* (49), 15548–15557. https://doi.org/10.1021/jacs.5b10748.
(74) Kotek, J.; Kálmán, F. K.; Hermann, P.; Brücher, E.; Binnemans, K.; Lukeš, I. Study of Thermodynamic and Kinetic Stability of Transition Metal and Lanthanide Complexes of DTPA Analogues with a Phosphorus Acid Pendant Arm. *Eur. J. Inorg. Chem.* **2006**, *2006* (10), 1976–1986. https://doi.org/10.1002/ejic.200501114.
(75) Táborský, P.; Lubal, P.; Havel, J.; Kotek, J.; Hermann, P.; Lukeš, I. Thermodynamic and Kinetic Studies of Lanthanide(III) Complexes with H_5Do3ap (1,4,7,10-Tetraazacyclododecane-1,4,7-Triacetic-10-(Methylphosphonic Acid)), a Monophosphonate Analogue of H_4Dota. *Collect. Czech. Chem. Commun.* **2005**, *70* (11), 1909–1942. https://doi.org/10.1135/cccc20051909.
(76) Grobner, T. Gadolinium--a Specific Trigger for the Development of Nephrogenic Fibrosing Dermopathy and Nephrogenic Systemic Fibrosis? *Nephrol. Dial. Transplant.* **2006**, *21* (4), 1104–1108. https://doi.org/10.1093/ndt/gfk062.

For Table of Contents Only

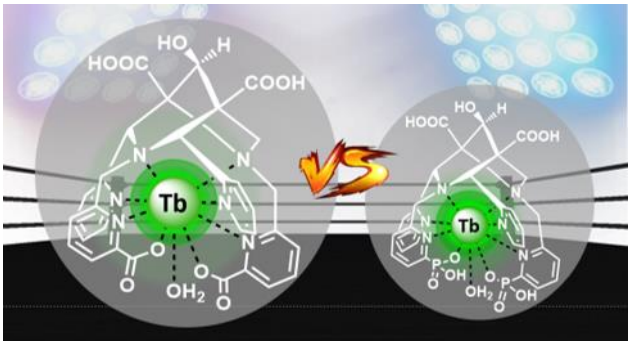

Small structural modifications in octadentate bispidine-based ligands lead to significant changes in the conformation of the diazabicyclononane skeleton, impacting protonation, Tb(III) complexation and complex stability. These findings provide valuable insights for designing more efficient luminescent Tb(III) complexes.